

Accepted manuscript doi: 10.1680/jphmg.21.00067

Accepted manuscript

As a service to our authors and readers, we are putting peer-reviewed accepted manuscripts (AM) online, in the Ahead of Print section of each journal web page, shortly after acceptance.

Disclaimer

The AM is yet to be copyedited and formatted in journal house style but can still be read and referenced by quoting its unique reference number, the digital object identifier (DOI). Once the AM has been typeset, an 'uncorrected proof' PDF will replace the 'accepted manuscript' PDF. These formatted articles may still be corrected by the authors. During the Production process, errors may be discovered which could affect the content, and all legal disclaimers that apply to the journal relate to these versions also.

Version of record

The final edited article will be published in PDF and HTML and will contain all author corrections and is considered the version of record. Authors wishing to reference an article published Ahead of Print should quote its DOI. When an issue becomes available, queuing Ahead of Print articles will move to that issue's Table of Contents. When the article is published in a journal issue, the full reference should be cited in addition to the DOI.

Submitted: 01 August 2021

Published online in ‘accepted manuscript’ format: 19 October 2022

Manuscript title: Testing Pile Foundations at the ETH Zurich Drum Centrifuge: Recent Developments

Authors: L. Sakellariadis¹, E. Bleiker¹, M. Iten¹, H. Buschor¹, A. Kieper¹, R. Herzog¹, A. Marin¹, O. Adamidis² and I. Anastasopoulos¹

Affiliations: ¹Institute for Geotechnical Engineering (IGT), D-BAUG, ETH Zurich, Switzerland and ²Department of Engineering Science, University of Oxford, UK; formerly IGT, ETH Zurich, Switzerland

Corresponding author: I. Anastasopoulos, Institute for Geotechnical Engineering (IGT), D-BAUG, ETH Zurich, Switzerland.

E-mail: ixa@ethz.ch

Abstract

Motivated by the need to develop rational design methods for the retrofit of existing bridges on pile groups, the paper introduces recent experimental developments at the ETHZ Drum centrifuge. Four setups are developed for vertical, pushover, combined, and vibration testing. Their capabilities and limitations are demonstrated using as example a 2x1 pile group on dense saturated sand. Single piles are subjected to vertical loading, exploring the role of installation effects and interface roughness. Pushover loading is employed to measure the moment capacity (M_{ult}) of a lightly- and a heavily-loaded group. In contrast to intuitive expectations, the heavily-loaded system mobilises larger M_{ult} . The developed combined loading apparatus is proof-tested for a shallow foundation. Combined loading under constant vertical load is conducted to derive failure envelopes, revealing significant coupling between lateral and moment loading, and confirming the expansion of the failure envelope with increasing static vertical load. The vibration testing setup is proof-tested, confirming the possibility to identify the natural frequency of the system and the small-strain stiffness of the foundation through non-destructive testing. Although the study is fuelled by our ongoing work on pile groups, the developed experimental setups are of general applicability for the study of deep and shallow foundation systems.

Keywords: Centrifuge modelling; Piles & Piling; Foundations; Bearing capacity; Stiffness; UN SDG 9: Industry, innovation and infrastructure

1. Introduction

Less common than geotechnical beam centrifuges, there are several drum centrifuge facilities around the world (Table 1). For a number of engineering applications, such as submarine landslides (Gue et al., 2010), debris flow (Yin et al., 2019), tsunami waves (Miyamoto et al., 2015), the drum centrifuge offers a significant advantage, as the model space is not constrained by lateral boundaries, being continuous around the channel. For foundation testing, in-flight pluviation allows the creation of uniform soil models, which can be used for parametric experimental investigations. Drum centrifuges are typically equipped with a centrally-installed tool platform, equipped with all the necessary tools, including actuators and measuring devices. The tool platform can be controlled independently from the drum channel, allowing for multiple tests at different locations along the circumference. An additional important feature is the possibility to completely stop the tool platform while the drum channel keeps spinning. With the help of a safety shield, this allows changing tools without spinning down, offering increased flexibility. Such features have been extensively exploited in the former 2 m diameter drum centrifuge of the University of Cambridge (e.g., Dean et al., 1997) and in the 1.2 m diameter drum centrifuge of the University of Western Australia (e.g., Gan et al., 2012), performing detailed parametric studies of foundations for offshore structures.

However, these major advantages of the drum centrifuge configuration come along with considerable challenges. Starting with model preparation, in-flight pluviation can be technically challenging and time consuming. Such in-flight procedure (e.g., Laue et al., 2001) requires dry sand pouring from the tool platform with a specially-designed revolving hopper, saturation and subsequent de-saturation of the model under enhanced gravity, followed by spinning down for scraping in order to create a levelled model surface, and finally spinning up again to conduct the test. In-flight installation of model structures and of the associated instrumentation would require advanced and precise robotics, while manual installation after spinning down the channel can be difficult in the confined space of the drum, leading to a risk of model disturbance or even collapse. Another practical issue is the significant amount of soil needed to fill the entire drum channel (about 2 tons for the ETH drum centrifuge), which makes the process of filling and emptying time consuming, but also physically demanding for the researchers and technicians involved.

In order to overcome some of these difficulties, parts of the circumference of the drum channel can be used to make smaller soil models. Moving one step further, smaller strong boxes can be used, prepared outside the drum under 1g conditions, and then mounted on the drum channel. In such a case, the drum centrifuge operation becomes similar to that of a beam centrifuge, with the caveat of the absence of a swing to allow for transition from 1g to *ng* conditions. This calls for a special procedure to keep the soil model stable, while rotating by 90 degrees to install on the stationary drum channel before spinning, which will be discussed later on. Such an approach is implemented herein to investigate the behaviour of piled foundations under different loading conditions.

The present study is motivated by the on-going upgrade of existing motorway infrastructure, which often requires the assessment and potential retrofitting of existing pile groups. One such example is the widening of existing bridges founded on piles to accommodate increasing traffic volume. Pile group strengthening to sustain the increased loads of the superstructure, can be a challenging, costly, and time-consuming operation, calling for optimised solutions. In Switzerland, the majority of existing bridges were built before the 1990s, with no seismic design considerations, while their current upgrade requires seismic assessment. Thus, a first pivotal element of retrofit design is the estimation of the moment capacity of the existing foundation.

Given the emphasis to existing structures (built mainly in the 60s and 70s), the efficiency of traditional bearing capacity methods needs to be carefully evaluated, calling for centrifuge model testing. Besides offering valuable insights on the mobilised resistance mechanisms of pile groups, centrifuge model testing is essential for validation of numerical models. Testing of pile groups at the ETH Zurich (ETHZ) drum centrifuge required the improvement and extension of established experimental procedures and the development of novel experimental setups. This paper summarizes these recent developments (during the past five years). Their capabilities, key technical aspects, challenges and limitations are thoroughly discussed using as example a fundamental, yet representative, 2 x 1 pile group on dense saturated sand, critically assessing their repeatability and reliability. Although the study is fuelled by our ongoing work on pile groups, the developed experimental setups are of general applicability for the study of deep and shallow foundation systems.

Prototype Problem

The simplified prototype problem used as the basis for the experimental campaign was carefully selected after developing and evaluating a database of existing road bridges in Switzerland (with the support of FEDRO), and is briefly outlined (Fig. 1):

- pile group layout: 2 x 2 (simplified to 2 x 1)
- pile diameter: $D = 1\text{ m}$
- pile length: $L = 15\text{ m}$
- spacing: $s / D = 3$
- installation method: bored
- resistance mechanism: end-bearing piles
- superstructure: rigid pier – $h = 12\text{ m}$

The testing campaign was divided in four phases, each one exploring different aspects of the behaviour of single piles and pile groups. In the first phase, single piles and pile groups are tested under vertical loading. The effect of the installation method and pile roughness on the bearing capacity and pull-out resistance of single piles is quantified. Furthermore, the role of group effects in function of pile spacing and the contribution the pile cap are further investigated. In the second phase, a simple single degree of freedom (SDOF) system founded on a 2 x 1 pile group is subjected to lateral pushover loading. Varying the concentrated mass (representing the bridge deck), the role of vertical loading on pile group moment capacity is investigated. The third phase involves combined horizontal and moment loading, under either constant vertical displacement or load. The fourth phase, consists of an exploratory non-destructive vibration test, aiming to experimentally measure the rocking stiffness of the tested 2 x 1 pilegroup. An overview of the experimental campaign is presented in Fig. 1.

The ETH Drum centrifuge facility

The centrifuge model tests were performed at 100g centrifugal acceleration, at the ETH Zurich (ETHZ) geotechnical drum centrifuge facility (Fig. 2). The facility was introduced 20 years ago by Springman et al. (2001) in the Inaugural Issue of the International Journal of Physical modelling in Geotechnics. Manufactured by Thomas Broadbent & Sons Ltd., the drum centrifuge can reach a maximum centrifugal acceleration of 440g carrying a payload of 2t. Figure 2 shows a plan view of the facility, along with a plan view and cross section of the drum centrifuge and its key components. The soil model is placed in the drum channel, while instrumentation and actuators can be installed both on the tool platform and on the channel.

The channel features an external diameter of 2.2 m, a height of 0.7 m and a depth of 0.3 m. By filling the entire channel at 440g, the model corresponds to a prototype problem of 132 m depth, 308 m width and 2.2 km length (Springman et al., 2001). However, strong boxes were used for the experimental series presented herein, as discussed in detail later on.

For the needs of each experimental setup (described in detail in the following sections), different devices and instruments were used, which are summarized in Table 2. For each experimental setup, appropriate computer programs were developed using NI LabView (National Instruments Corporation, 2003). The in-house developed data acquisition (DAQ) systems are delivered in modular form, permitting a flexible choice of sampling and recording modes. A total of 40 channels are available, allowing for measurement of different quantities during the experiments. The technical specifications of the actuators and of the equipment of the tool platform are documented in detail by Springman et al. (2001).

2. Model preparation: implemented solutions for controlled conditions

Model preparation is performed outside the centrifuge, using strong boxes. The sand layer is prepared via dry air pluviation using Perth Sand (Table 3), targeting dense homogeneous conditions ($D_r \approx 80\%$). As shown in Fig. 3a, the air pluviation setup consists of a cylindrical container with a hopper shape at the bottom, equipped with an adjustable opening. The sand is released through a rigid tube and a meshed disc into the strongbox. During this process, the container is hanging from a crane, moving in controlled meandering paths at constant velocity. The setup was first calibrated by adjusting the pluviation height and the opening size, selecting appropriate values for the target density (similar to Taeseri et al., 2018). The achieved relative density D_r of each test is verified using four pots per strongbox, placed at the bottom and the mid-height of the model, showing satisfactory repeatability (Fig. 3a). The sand at the target D_r was characterised through drained triaxial compression (CID) tests and constant normal load (CNL) interface tests at different confining stresses. The latter were performed for both smooth (aluminium) and rough (epoxy-sand coating) surfaces. Key results of the characterization tests are shown in Fig. 3b. With respect to the values of peak (φ'_{peak}) and constant volume (φ'_{cv}) friction angle (Table 3), the average values obtained for the four levels of confining stress are used in the calculations presented in the next sections.

A critical limitation of the drum centrifuge for the adopted model preparation method, lies on the need of the model to be rotated by 90° in order to be mounted onto the drum channel before spinning up, under unit gravity conditions (1g). To maintain the model stable during this process, the technique outlined by Morales et al. (2013) is employed, taking advantage of the apparent cohesion that develops in unsaturated sand. As schematically illustrated in Fig. 4, after completion of the air pluviation, the soil model is saturated and subsequently de-saturated. During this process capillary forces develop. Thanks to the grain distribution of Perth sand (fine – poorly graded), the apparent cohesion that develops due to suction is sufficient to ensure the stability of the soil specimen during installation, and for an adequate period of time prior to spinning of the centrifuge.

The described technique has been extensively implemented in previous centrifuge studies at ETHZ, investigating primarily shallow foundations (e.g., Arnold, 2005; Taeseri et al., 2018). In these previous studies, when the desired g-level was reached, the minimal amount of water remaining in the soil was allowed to drain. And since the mobilized failure mechanism is relatively shallow for such foundations, it was reasonably assumed that the apparent cohesion has practically vanished before the test. Such “dry” hypothesis was confirmed by Arnold (2005), who compared the load-settlement behaviour of a shallow footing on either dry or partially saturated soil (in-flight draining allowed), yielding very similar results (Fig. 5a). Such a verification was attempted for the problem studied herein for a single pile, jacked monotonically at 100g, unloaded and then subjected to vertical loading. As shown in Fig. 5b, the effect of partial saturation is proven to be non-negligible, with differences of about 20%.

In order to achieve fully controllable conditions, the tests are performed under full saturation. This required the development of an in-flight saturation system, the key components of which are shown in Fig. 5c. During spin-up and after reaching 20g, the two strong boxes and two additional water tanks are supplied externally with water. Since the free hydraulic height established with this process is not sufficient to completely fill the strong boxes, pumps are added to transfer the remaining amount of water from the tanks to the boxes. Solenoid valves are used to control the desired one-way flow. After the desired saturation is achieved (verified through PPT measurement and visually through the camera), spinning up continues to the target g-level (100g) and the test is conducted. After its completion and prior to spin-down, the valves are opened to allow draining, re-establishing partial saturation to prevent

collapse of the model upon full stop. The components of the in-flight saturation system are symmetrically installed and connected in parallel (shown in the bottom connectivity sketch of Fig. 5c) for enhanced redundancy. Pore pressure transducers are used to monitor the process.

3. Vertical loading

Centrifuge modelling has been employed to better understand the load transfer mechanisms and evaluate widely used design approaches (e.g., De Nicola & Randolph, 1997; Fioravante, 2002; Lehane et al., 2005). The construction method is recognized to significantly affect axial bearing capacity and load–settlement response of piles (e.g., Fleming et al., 2008, Viggiani et al., 2014). Piles are broadly categorized according to the installation method (bored, jacked or driven) and the construction material (steel, concrete, wood). Both factors affect significantly their shaft and tip resistance. Their effect is quantified herein by testing different pile–soil interfaces and installation methods, as follows:

(i) Monotonic jacking (MJ) at 1g

The piles are jacked monotonically at a rate of 0.5 mm/s at 1g, before spinning. Since the stress increase during penetration can be assumed negligible compared to the stresses that develop at 100g, the piles can be reasonably considered as “wished-in-place”. Despite local densification that also takes place during 1g installation, this method is considered appropriate for the simulation of bored piles (Madabhushi, 2014).

(ii) Monotonic jacking (MJ) at 100g

The piles are jacked monotonically at a rate of 0.5 mm/s at 100g. This method mimics the installation of jacked piles in the field, in a simplified manner.

(iii) Cyclic jacking (CJ) at 100g – “Load controlled (LC)”

The piles are installed in a series of jacking strokes at 100g. For each stroke, they are pushed by 5 mm (model scale) at a rate of 0.5 mm/s, followed by load release at the top of the pile (load controlled). This method offers a more realistic simulation of jacked piles in the field.

(iv) Cyclic jacking (CJ) at 100g – “Displacement controlled (DC)”

The piles are installed in a series of jacking strokes at 100g. For each stroke, they are pushed by 5mm (model scale) at a rate of 0.5 mm/s, followed by a reversal of the applied displacement by half of the downward stroke (displacement controlled). This “pseudo-dynamic” installation method was introduced by Lehane & White (2005), with the extraction component aimed at simulating the rebound experienced by driven piles. This approach is

targeting driven piles, as a simpler alternative to the more accurate but challenging in-flight impact driving method (e.g., De Nicola & Randolph, 1994).

In all methods, after completing the installation phase, the applied load is released. Subsequently, the static bearing capacity and pull out test is conducted. With respect to the soil-pile interface, the two extremes are tested: smooth, using aluminium piles; and rough by adhering sand on the roughened aluminium surface, using epoxy resin. In the rough piles, the external diameter of the solid section is intentionally selected to be 3 mm smaller than the target diameter (10 mm), accounting for the epoxy-sand layer. The interface behaviour is investigated through constant normal load (CNL) interface tests. In both cases, the effective diameter of the model piles is maintained at $D = 10 \text{ mm}$ (corresponding to 1 m in prototype scale). Solid aluminium piles are used to avoid any potential buckling problems during in-flight installation. An overview of the experimental setup used is shown in Fig. 6a.

Preliminary testing of the piles rigidly mounted on the actuator revealed a small imbalance during spin-up, resulting to movement of the tool platform relative to the channel, subjecting the piles to compression on one side and tension on the opposite side. To minimize such undesired movements, the tool platform was rigidly connected to the channel using stiffeners. A laser sensor is mounted on the actuator targeting the strong box, monitoring precisely the achieved pile displacement. Moreover, a linear slider of limited gap (Fig. 6a, b) is introduced between the piles and the actuator to accommodate small parasitic relative movements of the tool platform. The slider is also essential to allow the piles to settle together with the soil during spin-up, preventing the development of negative skin friction. An unavoidable limitation of this setup is a small initial loading of the piles due to the slider's self-weight. The piles are equipped with a pair of strain gauges at the tip, as shown in Fig. 6c.

This setup was successfully implemented for a total of eight centrifuge tests (Table 4). The first four simulated single piles, where it was feasible to test multiple installations per box. Maintaining a spacing $s/D = 10$ (100 mm in model scale) between the each pile installation and the boundaries, the disturbance according to Bolton et al. (1999) is expected to be minor. In the remaining four tests, each box was used to test simultaneously a 2 x 1 rough pile group installed at 1g (bored), varying pile spacing and engaging the pile cap to explore group effects.

Installation effects on smooth and rough single piles

Key test results of single pile subjected to vertical loading are summarized in Fig. 7. Unless otherwise stated, the results are discussed in prototype scale. Figures 7a,b compare the load–settlement response of smooth and rough piles. The comparison is performed first for the entire experiment, including the installation phase, and then focusing on the recorded response after the end of the installation. In the first case, the settlement w is normalized to the pile length L , while in the second the pile diameter D is used for normalization. As expected, the in-flight installation increases significantly the bearing capacity and pull-out resistance of both smooth and rough piles.

The results are summarised in Table 5, where the bearing capacity under compression is defined conventionally as the load corresponding to settlement equal to 10% of pile diameter, while the pull-out resistance corresponds to the maximum value obtained. To quantify the effect of the installation method, the behaviour of the bored (1g-MJ) pile is used as reference. The in-flight installation of rough piles increases the bearing capacity and the pull-out resistance by a factor of 4.4 to 5.8 and 2.1 to 3.8, respectively. In the case of smooth piles, the effect of the installation method is even more pronounced, increasing the bearing capacity by a factor of 5.8 to 6.6, and the pull out resistance by 3.2 to 4.6. The *LC* installation mobilised the highest bearing capacity, while both cyclic approaches mobilise higher resistance than the monotonic installation, both in bearing capacity and pull-out resistance.

A key element of this study is testing and evaluating the reliability of the implemented experimental procedures. For this purpose the monotonic installations (1g and 100g) were performed simultaneously on both strong boxes. The comparison between the two sides is presented indicatively for rough piles in Fig. 8, showing very satisfactory repeatability.

The results are further compared to similar centrifuge studies. Burali D'Arezzo et al. (2014) compared in-flight monotonic jacking to *LC* and *DC* cyclic jacking. They observed that *LC* installations yield similar load to monotonic ones, while with few exceptions, *DC* showed lower loads for both smooth and rough piles. The rough interface led to 50% higher load. On the contrary, Haffar et al. (2017) documented centrifuge test results on rough piles, comparing monotonic to *LC* installations of variable stroke cycles. In their case, the monotonic installation mobilised the largest bearing capacity, but the lowest pull-out resistance. Both of these studies are in partial agreement with the results presented herein. It is therefore not possible to deduce a general conclusion on which installation method

mobilises higher resistance. The latter appears to be sensitive to soil conditions, calling for further testing.

The results of the current study are also compared to bearing capacity theory. The applicability of traditional approaches to pile foundations has received some scepticism over the past decades (e.g., Fellenius, 1999). Modern design codes use partial safety factors, reducing the capacity estimated by bearing capacity theory, promoting empirical correlations based on in-situ soil testing (e.g., CPT). The key assumption of bearing capacity theory (i.e., mobilisation of an ultimate shear mechanism at the pile tip) is not supported by field observations. Both large and small scale tests of piles in sand do not show a tendency of reaching asymptotically a limit resistance, even for settlement much in excess of 10% of pile diameter. Figure 8 shows the point at $w/D = 0.1$, which is conventionally defined as bearing capacity. After reaching this point, the pile resistance keeps increasing with settlement w .

Despite the limitations of bearing capacity theory, it is undeniable that the design of many of the existing foundations was based on such an approach. To that end, the evaluation of such methods remains important. The bearing capacity solution is obtained for our problem using the soil parameters of Fig. 3. The estimation of tip and shaft resistance follows Eqs. 1 and 2:

$$V_{tip} = \pi D^2 N_q \sigma'_{v(tip)} \quad (1)$$

$$V_{shaft} = \pi DL K \tan \delta \sigma'_{v(L/2)} \quad (2)$$

The criticism mainly lies in the remarkable variability of N_q proposed by different authors, for a given friction angle ϕ . The selection of ϕ for dense sand is a challenge by itself. In the current study, the N_q proposed by Berenzansev (1961) is adopted (Fleming et al., 2008, Viggiani et al., 2014). Regarding ϕ , two approaches were followed. First, the iterative process proposed by Fleming et al. (2008) is applied, accounting for sand dilatancy (Bolton, 1986). A second more conservative estimate is obtained by using the critical state friction angle. The calculated values correspond to driven piles and is reduced by 70% for bored piles (Fleming, 2009).

With respect to the shaft resistance, applying the β -method the variation is significantly smaller. The values of earth pressure coefficient K proposed by Fleming (2009) and Poulos (2017) are adopted, covering the range found in the literature. The comparison presented in Fig. 8 shows the sensitivity of the capacity obtained by bearing capacity theory on the assumptions made, even for the idealised and well documented problem studied herein. The calculated bearing capacities are found to be conservative for the cases examined herein, but this conclusion cannot be generalized. At this point, it should be noted that grain crushing was observed in our experiments (Fig. 8), when the piles were installed in-flight, which is not accounted for in the previous calculations.

The behaviour of the model piles is further elucidated by decomposing the total resistance into shaft and tip resistance, by means of the instrumented pile-tip. Figure 9a shows the total, tip and shaft resistance of *smooth* piles jacked monotonically at 1g (left, corresponding to bored piles) and 100g (right, corresponding to jacked piles). The same results are presented for the *rough* piles in Fig. 9b. The effect of pile roughness can be deduced by comparing the results of Figs. 9a and 9b. Pile roughness leads to an increase of the total resistance by 65% and 26%, for 1g and 100g installation, respectively. Under 1g installation, pile roughness leads to an increase of tip and shaft resistance by 16% and 154%, respectively. In the case of 100g installation, pile roughness led to an increase of shaft resistance by 260%, but no increase was observed for the tip resistance, as it should be expected according to Borghi et al. (2001). However, inspection of the pile after the test revealed that the epoxy-sand coating at the tip did not fully sustain the load during installation (partially sheared off), which explains this contradictory result.

Group effects – definition of reference model

Group effects and the contribution of the pile cap are investigated by testing the prototype 2 x 1 bored pile group. A rough soil-pile interface is considered, and the installation is performed under 1g conditions. As previously, after reaching the target 100g level, the pile group is subjected to vertical push-down, followed by pull-out. The effect of pile spacing is studied by varying the normalized pile spacing s/D from 2 to 4, covering the range typically encountered in practice. As shown in the vertical force–normalized settlement ($V - w/D$) response of Fig. 10a, the closely spaced piles ($s/D = 2$) experience limited increase in terms of push-down response, which is observable for large settlements ($w/D > 0.1$), and a small reduction in terms of pull out resistance. No group effects are observable for larger pile

spacing ($s/D = 3$ and 4), with a small exception in the pull-out response. The limited presence of group effects, even for $s/D = 2$, is related to the very fundamental 2×1 pile group layout, and should by no means be generalised to larger pile groups.

The role of the pile cap is examined in Fig. 10b. The centrifuge model test is repeated, but this time the pile cap is installed a bit lower, so that it gains full contact with the foundation soil when the pile group is jacked to the desired depth (before spin-up). Although the contribution of the pile cap is certainly non-negligible, its engagement starts becoming visible in the push-down response for relatively larger settlement, $w/D > 0.15$. This is partially attributed to unavoidable soil disturbance in the area of the cap during 1g installation. In all tests, some hairline cracks could be observed on the ground surface after the 1g installation process (during which the model is still partially saturated), which always disappeared after spin-up and in-flight saturation, but some disturbance close to the ground surface is still possible. Furthermore, during the spin-up process, the settlement of the model piles is expected to be lower than that of the surrounding soil leading to some development of negative skin friction. The latter also explains the relatively late full engagement of the pile cap. The conventionally defined bearing capacity (i.e., for $w/D = 0.1$) from this test is used to define the factor of safety against purely vertical loading for the lateral pushover tests.

At this point, some unavoidable limitations of centrifuge model testing should be spelled out. The experimental results are presented in prototype scale and compared to traditional bearing capacity approaches. However, despite satisfying the recommendations regarding pile diameter to grain size ratio (Bolton et al., 1999; Fioravante, 2002), the extrapolation of the results to prototype conditions is not totally immune to scale effects. The latter are primarily related to the shaft resistance of the model piles. As revealed by the centrifuge studies of Fioravante (2002) and Lehane et al. (2005a;b), the average mobilised peak shaft resistance decreases with the increase of pile diameter. This was attributed to the volumetric response of the interface shear zone, which was successfully reproduced by combining cavity expansion theory and constant normal stiffness (CNS) interface tests. The same effect was observed numerically by Loukidis & Salgado (2008). However, it was concluded that the effect of interface dilation is limited in full scale piles; it is only of significance when the pile diameter is similar to the thickness of the interface shear zone ($\approx 5D_{50} = 1 \text{ mm}$). Therefore, the presented centrifuge model test results should be expected to over-predict the ultimate shaft resistance of the prototype.

An additional limitation of the experimental results lies in the limited dependence of the displacement required to mobilise the peak shaft resistance to pile diameter. In the pull-out tests (Figs. 7, 8, 10), the peak resistance is mobilised at about 2 mm (similar to the CNL tests, Fig. 3). When converted to prototype scale, this corresponds to 200 mm, which cannot be considered realistic and is not in accord with full scale test results (e.g. Ismael, 1989). Since the displacement required to mobilise shaft resistance is a function of the thickness of the developing interface shear zone (which is a function of grain size, expressed through D_{50}), it should be of a similar order of magnitude in the full scale piles. Since the grain size in the centrifuge model tests cannot be reduced, such scale effects are practically unavoidable, and should be kept in mind when evaluating and interpreting the experimental results.

4. Lateral pushover loading

Being common practice in structural seismic design, lateral pushover loading has also been used for shallow foundations (e.g., Gajan et al. 2005; Anastasopoulos et al. 2012). With respect to pile groups, most centrifuge studies have focused on purely lateral loading. However, when considering the seismic response of bridges on pile groups (which are typically characterized by a relatively large slenderness ratio), the overturning moment is the one that is critical for seismic response. To the best of our knowledge, there are no documented centrifuge pushover tests on such slender structures founded on pile groups.

When a centrifuge model of pile group is to be subjected to lateral loading, a key element is the selection of an appropriate material and section geometry of the model pile, targeting the bending stiffness of the prototype problem. Considering the centrifuge scaling laws, matching both the bending stiffness and the moment capacity of the prototype reinforced concrete (RC) piles is challenging. Recent efforts to reproduce the quasi-brittle behaviour of concrete in scaled models can be found in the recent literature (Knappett et al. 2011; Loli et al. 2014; Zhao et al., 2021). Despite the very encouraging results of these studies, given the unavoidable uncertainties in fully characterizing the response of such models, and considering the 1:100 scale factor of the experiments conducted herein, it was decided to follow a more conventional approach. The model piles are made of aluminium (H14) with hollow circular section ($D = 7\text{ mm}$, $t = 0.45\text{ mm}$). The external diameter is intentionally selected to be 3 mm smaller than the target diameter (10 mm), accounting for the epoxy-sand layer required to achieve a rough interface (appropriate for bored piles). It should be pointed out, that the epoxy layer has a non-negligible effect in both the capacity and stiffness of the

model pile, and should be accounted for in the selection of the aluminium tubes used to model the piles.

The model piles are intended to match the bending stiffness of the 1 m diameter RC piles (concrete class C25, steel class S500) of the prototype, considering a longitudinal reinforcement ratio of 1% (typical, especially for older piles) and the minimum allowable transverse reinforcement. Subjected to moment loading, the piles develop axial forces, leading to an increase and a reduction of the axial force of the leading and trailing pile, respectively. Therefore, the selection of the reference behaviour of the prototype piles should account for the axial load dependency of the moment–curvature response of the prototype RC piles. On the other hand, the stiffness of the epoxy-coated aluminium model piles is expected to be independent of axial loading. Hence, the selection of model pile geometry was made by comparing the response to that of the prototype, for the entire range of expected axial pile loads, considering a representative factor of safety against purely vertical loading $FS_v = 3$. The latter is achieved by adjusting the superstructure mass, on the basis of the previously discussed axial loading tests.

The model piles are verified through cantilever beam tests and three-point bending tests, with and without the epoxy coating. The latter is necessary for the connection between the piles and the cap, while the first corresponds to the free length of the pile, where the epoxy layer is present. Both testing approaches yield similar results. The three-point bending tests (2 tests with and 2 tests without epoxy) are documented in Fig. 11a, revealing the non-negligible effect of the epoxy layer, both in terms of capacity and stiffness. The behaviour of the model piles is then verified against section analysis of the prototype RC piles. Figure 11b compares the measured force-displacement ($F - \delta$) response of the epoxy-coated aluminium model pile to section analysis of the prototype RC pile, considering the entire range of axial loading, from the initial static condition to the maximum and minimum axial forces expected to develop during moment loading. The selected model pile offers a reasonable matching of prototype bending stiffness, for the range of axial forces considered. This is not the case for the pile bending moment capacity, which cannot be properly scaled in this manner, being significantly overestimated. This should be considered in the interpretation of the test results.

As shown in the experimental setup of Fig. 12, a single degree of freedom (SDOF) system is employed for the lateral pushover tests, comprising the 2 x 1 pile group with the epoxy-coated aluminium piles, a rigid pier and pile cap, and a concentrated mass (representing the bridge superstructure). Two masses are considered, one corresponding to a representative safety factor ($FS_v = 3$), and a heavier one that represents a deck widening scenario without any foundation retrofitting ($FS_v = 1.5$). The latter is not necessarily realistic, but was intentionally selected to explore the lateral pushover response of an overly heavily-loaded pile group. As summarized in Table 5, three lateral pushover tests were conducted, as the lightly-loaded ($FS_v = 3$) pile group was tested twice for repeatability assessment.

The pile group is installed (jacked) at 1g conditions prior to spin-up, which is representative of the bored piles of the prototype. Then, the superstructure (rigid pier – mass assembly) is mounted onto the foundation, using an appropriate support to undertake the weight of the model due to the 1g component, avoiding soil disturbance. The support is positioned at the centre of the concentrated mass, using low-friction Teflon tape between the two parts. The support is equipped with a magnet, which is activated after carefully positioning the superstructure model. This limits model disturbance while fixing the superstructure to the foundation using four screws (Fig. 12). While spinning up to 20g, the magnet is deactivated and the superstructure is free to settle along with the soil. The support can be totally removed using a linear actuator, but it was decided to remain in place in order to undertake the 1g component (which is a peculiarity of the drum centrifuge setup) throughout the entire test.

After reaching the target 100g level, the static monotonic pushover tests are conducted. All tests are displacement-controlled with a rate of 0.02 mm/s to avoid undesired rate effects. The target displacement is applied at the centre of mass through a sliding hinge connection. The latter is crucial in allowing the system to experience freely uplifting or sinking response. The applied load is measured using a load-cell mounted to the actuator arm, while the horizontal, vertical and rotational movement of the model is monitored throughout the test using a system of three laser sensors mounted on the strong box (Fig. 12). The experimental results are expressed in terms of force-displacement ($H - \delta$), moment-rotation ($M - \theta$), and settlement-rotation ($w - \theta$) response in Fig. 13.

Figure 13a compares the two models in terms of force–displacement ($H - \delta$) response. The results (prototype scale) reveal that the heavily-loaded ($FS_v = 1.5$) pile group exhibits higher initial stiffness and almost 25% higher lateral capacity than the lightly-loaded ($FS_v = 3$) system (1.9MN as opposed to 1.5MN). In both cases, the ultimate load is reached at approximately 1 m of applied displacement. Multiplying the force by the pier height, and using both horizontal laser records, the moment–rotation ($M - \theta$) response of Fig. 13b is derived. The latter includes second-order effects (more pronounced for the heavily-loaded system), which are removed in Fig. 13c. The heavily-loaded pile group mobilises 45% larger moment resistance. Looking at the lateral displacement atop and at the base reference point (Figs. 13d,e), both systems experience the same ratio of (non-negligible) horizontal displacement to rotation. The pole of rotation is about 6 m below the reference point for both cases.

The response is considerably different in terms of settlement–rotation ($w - \theta$) response. As shown in Fig. 13f, the lightly-loaded ($FS_v = 3$) system initially settles, but subsequently exhibits an uplifting response, while the heavily-loaded ($FS_v = 1.5$) systems sustains a sinking dominated response. By comparing the response of the two systems, it is also possible to approximately estimate the additional static settlement due to the increase of the vertical load (deck widening), which reaches 0.07 m. This is only an approximation, as the entire soil model settles during spin-up; a more accurate estimate would require measurement of the free-field settlement, as well. Regarding the repeatability assessment, the results are quite similar (dashed vs. solid line), increasing our confidence in the experimental procedure.

Pile design against lateral loading typically considers the overturning moment being undertaken by compressive and tensile forces of the leading and trailing piles, respectively. This approach conveniently treats the applied moment as an eccentric vertical load, ignoring the additional moment that develops due to lateral pile loading and the coupling of the two resistance mechanisms (Di Laora, 2019; FEMA, 2009). The centrifuge test results are used to assess the validity of this approach. Instead of bearing capacity theory, the moment calculation uses the measured ultimate vertical pile loads.

Figure 14a shows the expected vertical load path of the leading and the trailing piles, for the lightly- and heavily-loaded pile group. The contribution of the pile cap is ignored, and therefore the two piles need to be further compressed or unloaded by an equal amount (dV) to maintain vertical equilibrium. Since the leading pile (under compression) mobilises more-

and-more resistance with increasing penetration, the ultimate limit state is reached when the pull-out capacity of the trailing pile is fully mobilized. After this point, no further moment resistance can be mobilised through axial pile loading. The unloading (uplift) load path shown in Fig. 14a is derived by shifting the experimentally measured curve (AB) to the point that corresponds to the initial vertical load (A') due to static loading. In this way, the settlement, rotation (w, θ) of the pile cap at the ultimate limit state (ULS) can be calculated, explaining the uplifting and sinking tendency of the lightly- and of the heavily-loaded group, respectively. As shown in the figure, for the lightly-loaded ($FS_v = 3$) system, at ULS the leading pile settles by -0.1 m and the trailing pile uplifts by 0.3 m, leading to the previously discussed uplifting-dominated response. In stark contrast, for the heavily-loaded ($FS_v = 1.5$) system, ULS is reached with the leading pile settling by -0.45 m and the trailing one uplifting by 0.4 m, leading to a sinking-dominated response.

The moment-rotation ($M - \theta$) response can be predicted considering only the vertical load paths of the piles, maintaining vertical equilibrium. The result of such calculation is compared to the experimental results in Fig. 14b. The estimation of the ultimate moment capacity (M_{ult}) is quite conservative, underestimating the experimental results by 51% and 40% for the lightly-loaded and the heavily-loaded system, respectively. A better prediction can be achieved when the bending moment capacity (M_y) of the model piles is added to the calculation, assuming the development of plastic hinges at the pile cap level. This hypothesis is used only as a simplification, as it does not comply with the observed response, where the plastic hinges developed deeper. The prediction of the initial rocking stiffness (K_r) is reasonably good for the lightly-loaded system, but rather poor for the heavily-loaded. Due to its increased initial static loading ($FS_v = 1.5$), the leading pile has already mobilized a larger portion of its axial bearing capacity, being drawn deeper into its nonlinear regime. As a result, when subsequently subjected to moment loading, it exhibits softer axial response. And since the calculation only accounts for axial pile loading, the heavily-loaded system exhibits softer $M - \theta$ response compared to the lightly-loaded. However, the experimental results show the exact opposite trend: the heavily-loaded pile group exhibits larger initial rocking stiffness.

Despite its key role, the axial loading mechanism is not sufficient to reproduce the observed behaviour, both in terms of ultimate moment capacity (M_{ult}) and rocking stiffness (K_r). Despite using the *measured* axial load–settlement response (avoiding the uncertainties of bearing capacity calculations), the differences to the observed rocking behaviour are non-negligible. The contribution of the lateral loading mechanism (pile bending) and the additional resistance offered by the pile cap appear to be important, calling for further investigation and deeper understanding. The overestimation (compared to the prototype problem) of the bending moment capacity (M_y) of the piles is a limitation of the experiments; its effect will be quantified in a forthcoming publication through numerical analysis. The coupling between lateral and moment loading is assessed in the next section, by subjecting the pile group to combined (*VHM*) loading.

5. Combined (*VHM*) loading

In the previous section, the 2 x 1 bored pile group was tested under pushover loading, offering useful insights. Despite its significance in the realm of pseudo-static foundation design, only a single $M - H$ path is possible through pushover loading, being a function of the height of the SDOF system. Applying different load paths would require different parts to be manufactured. Most importantly, each pushover test can only yield a single failure point in the 3D load space. An alternative setup is developed, allowing different types of displacement-controlled (with the potential of extending to force-controlled) combined (*VHM*) loading tests.

Constant vertical displacement tests (Swipe tests)

The swipe-testing approach has been applied extensively (experimentally and numerically) to derive combined loading yield surfaces of various foundation schemes, especially for offshore applications. Introduced by Tan (1990), the “side-swipe” test was based on the analogy between undrained triaxial testing of pre-consolidated samples and lateral displacement testing of vertically-preloaded foundations, under conditions of zero settlement and rotation. The load path of such a test was argued to closely track the yield surface in the $V - H$ load space, for a given foundation penetration. Varying the ratio of horizontal displacement (u) to rotation (θ), a limited number of swipe tests is sufficient to generate the 3D yield surface. Such a representation of admissible combined loads was proposed since the late 70s (Ticof, 1977) to overcome the shortcomings of the traditional bearing capacity

approach (Terzaghi, 1943), which uses modification factors for load inclination and eccentricity.

Swipe testing requires two steps (Gottardi et al., 1999). First, the foundation is loaded purely vertically to a prescribed load. If the test aims to explore the yield surface at low vertical loading, the foundation is then unloaded to the selected level. In both cases, after the desired load is reached, vertical displacement is held constant. At the second step, the foundation is subjected to a “swipe path” of selected u or/and θ (keeping the vertical displacement constant). Successful execution requires good control of the in-plane vertical, horizontal and rotational movements. Different apparatuses have been developed for this scope, either for 1g testing (Martin, 1994) or for centrifuge (ng) testing (e.g., Dean et al., 1997). A summary of various such developments can be found in Zhang et al. (2013).

The developed experimental setup is depicted in Fig. 15. The control of all in-plane displacements is achieved by simultaneous coordinated movement of three actuators, as shown in Fig. 15a. A key component of the developed assembly is the actuator mounted on the tool platform, which has two degrees of freedom (allowing very precise vertical and horizontal movements) and was used for the vertical loading tests. The other two actuators are mounted on the strong box and are the same with the ones previously described for the pushover tests. These actuators were customised in-house at ETHZ, replacing the built-in brushless motor with a stepper motor for adequately slow and precise movements at 100g conditions. The actuators are connected through a mechanical assembly, consisting of rigid aluminium parts and two hinges (roller bearings for reduced friction). The definition of the reference point requires four setup parameters: l_1, l_2, r_1, r_2 (Fig. 15b). In order to impose any desired displacement path (horizontal δ_x , vertical δ_y , and rotational $\delta\theta$), the tool platform actuator needs to move horizontally on the x-axis (δx_{tp}), either extending or contracting along the y-axis (δl_{tp}). The two actuators mounted on the strong box either need to contract or extend ($\delta l_1, \delta l_2$). The coordinated movement of the three actuators is achieved following Eqs. 3 – 6, which are implemented in a computer program, developed using NI LabView:

$$\delta x_{tp} = \delta_x + r_1 * \sin(\delta\theta) \quad (3)$$

$$\delta L_{tp} = r_1 * (1 - \cos(\delta\theta)) - \delta_y \quad (4)$$

$$\delta L_1 = \sqrt{(\delta_x + r_1 * \sin(\delta\theta) + l_1)^2 + (\delta_y + r_1 * \cos(\delta\theta) - r_1)^2} - l_1 \quad (5)$$

$$\delta L_2 = \sqrt{(\delta_x + r_2 * \sin(\delta\theta) - l_2)^2 + (\delta_y + r_2 * \cos(\delta\theta) - r_2)^2} - l_2 \quad (6)$$

Each actuator is equipped with a pair of load cells and laser sensors. The measured displacements are further used in a proportional integral derivative (PID) control loop feedback mechanism, ensuring that the coordinated movement closely follows the target path.

In addition to the combined loading assembly (side A), Fig. 15c also shows the symmetric side B. The strong boxes are filled in exactly the same way to maintain balance of the drum channel. However, this is not sufficient to ensure balance during the test. Considering the swipe test sequence, the applied vertical load (V) initially increases, until the desired value is reached. In the swipe phase, V reduces continuously as the load path is tracking the yield surface. In the absence of a counter force on side B, such load changes may lead to movement of the platform relative to the channel, introducing errors. To ensure balance during testing, the symmetric tool platform actuator (side B) is rigidly fixed to the strong box, and is constantly regulated to maintain the same load with side A. Furthermore, mechanical stiffeners are used to minimize any tendency of movement of the tool platform relative to the channel. Such movements were monitored during testing, confirming the efficiency of the balance system. The importance of balance control in deriving high quality experimental data was pointed out by Zhang et al. (2013), regarding the VHM apparatus developed at the UWA drum centrifuge.

The developed experimental setup is proof tested using the simpler problem of a shallow 40mm square foundation, similar to the pile cap of the studied 2 x 1 pile group. Sand is glued at the bottom of the footing to achieve rough conditions; the reference point (RP) is selected at its base. Two side-swipe tests were conducted for the purposes of this study (Table 6) and key results are presented in Fig. 16. The only difference between the two tests lies on the sidewalls of the footing, which were removed in the second test. Conducting similar 1g swipe tests, Gottardi et al. (1999) argued that the sidewall resistance is rather small, a hypothesis that is confirmed by our tests. Interestingly, at 100g (this study) full mobilisation of bearing capacity requires penetration $w/B \approx 15\%$ as opposed to $w/D \approx 2 - 3\%$ for the 1g tests of Gottardi et al. (1999). Despite this difference in required penetration, the mobilised moment is similar; the horizontal resistance is not affected by the sidewalls (Fig. 16).

Certain limitations of the experimental setup were observed during the first step of the test (vertical penetration), during which limited (but not negligible) horizontal and moment resistance was mobilised. Furthermore, after the desired penetration is reached and the vertical movement is halted, limited relaxation of the vertical force is observed (Fig. 16).

Such tendencies have been observed in similar centrifuge studies (Zhang et al., 2012; Cheng & Cassidy, 2015). Despite these limitations, the result of the swipe test is considered successful and in good agreement with similar studies and with the failure envelope proposed by Gottardi et al. (1999) for maximum horizontal force $H_0 = 0.12V_0$:

$$\frac{H}{H_0} = 4 \frac{V}{V_0} \left(1 - \frac{V}{V_0}\right) \quad (7)$$

The developed combined loading setup offers very promising results, but more tests are required to fully explore its capabilities. The possibility for swipe testing of the studied pile groups was carefully considered, but certain challenges were identified, necessitating its adaptation. First, the PVC ring needed for full model saturation (Fig. 11) doesn't fit with the pile group model. Most importantly, the connection of the tool platform actuator to the assembly requires precise positioning in order to avoid disturbance of the model, as the pile group is already installed at 1g. In addition, with the current assembly, the development of negative skin friction during spin-up is unavoidable, since the piles are not allowed to freely settle. Therefore, to proceed with pile group testing, it was decided to simplify the setup, performing constant vertical load tests, as discussed in the following section.

Constant vertical load tests

The models used previously for lateral pushover loading are subjected herein to combined loading under constant vertical load, employing the experimental setup of Fig. 17. Similarly to the pushover tests, a concentrated mass is used to adjust the vertical load, using the pair of actuators of the VHM loading setup to apply the desired horizontal or/and rotational movement. Sliding hinge connections are employed to allow settlement and uplifting.

As summarized in Table 6, five tests were performed with this setup, testing the lightly- and the heavily-loaded pile group, as in the pushover tests. The two models are subjected either to horizontal (u) or rotational (θ) movement at the reference point. In the first case, the foundation is subjected primarily to horizontal loading (representative of short piers), while in the second case the applied moment is dominant (representative of slender, rocking dominated systems). The applied load paths are shown in Fig. 18, along with those of the previously discussed pushover tests. In the absence of a regulation control loop in these tests, small parasitic rotations or horizontal displacements were observed, which can be noticed in the deformed shape of the models.

Figure 18 summarises the three load paths imposed to the lightly-loaded ($FS_v = 3$) and the heavily-loaded ($FS_v = 1.5$) pile group. Despite the limited number of failure points (3 per FS_v), it is possible to get a first picture of the failure envelope at each level of vertical loading. Similarly to the results of pushover loading, when subjected primarily to moment loading (load path 1), the heavily-loaded pile group mobilises higher resistance. Since pull-out failure of the trailing pile is critical, the more heavily-loaded system has a clear potential of mobilizing larger moment through axial loading. Compared to the pushover loading (load path 2), both systems mobilise significantly larger moment resistance: 35% and 65% higher for $FS_v = 1.5$ and 3, respectively. This impressive difference is indicative of the importance of coupling between lateral load and overturning moment, which is typically neglected in practice. Subjected to primarily horizontal loading (load path 3), the lightly-loaded pile group mobilises 11% higher resistance. This can be attributed to the reduced initial shear deformation of the soil, or to the variability of the bending moment capacity of the model piles, which will be discussed later.

Using the ultimate load points, linear trend lines are drawn to qualitatively illustrate the failure envelopes in the first quadrant of the $M - H$ space (Fig. 18). The effect of lateral loading on the moment resistance of the studied moderately tall ($h = 12\text{ m}$) pier is non-negligible. Looking at the failure mechanisms, load paths 1 ($u = 0$) and 2 (pushover) result in the formation of a single plastic hinge at the model piles. Both in the leading and the trailing pile, the depth of the plastic hinge increases with the increase of the lateral loading component (load path 2 vs. 1). When the pile group is mainly subjected to lateral loading ($\theta = 0$), two plastic hinges are formed at both piles (load path 3), similar to the postulated mechanism of the widely used Broms (1964) theory, for fixed head conditions. The extrapolation of the experimental results to the prototype problem is not totally straight forward. In addition to the previously discussed scale effects, failure would take place earlier in the prototype, as the model piles overestimate the bending moment capacity of the prototype RC piles (Fig. 12).

The behaviour of the model piles under lateral loading is further investigated through an additional test, where the lightly-loaded pile group is loaded laterally out of plane. In this way, the response of two equivalent “single” piles is measured. The results are presented in Fig. 19, where the measured force is averaged and compared to the prediction of Broms (1964) theory for fixed-head laterally loaded single piles. The latter is known to

underestimate by up to 30% the resistance when compared to field tests, while the limit soil pressure proposed by Barton (1982) gives better estimates (Fleming et al. 2008). This is confirmed by the experimental result, which is indeed in good agreement with the solution of Barton. In both approaches, the peak friction angle used to estimate the passive earth pressure coefficient, K_p , is an average value of the triaxial test results of Fig. 3. Regarding the bending moment capacity of the model piles (M_y), the average value the of 3-Point bending tests on piles with and without epoxy-sand coating is used (Fig. 12). The epoxy-sand coating results in 15% variation of M_y of the model piles. This variability is also observable in Fig. 19, as it affects the depth of the second (lower) plastic hinge, which ranges from 3.9 m to 4.4 m. Both values are slightly lower than the prediction of Barton ($f = 4.9\text{ m}$).

Summarising, the observed failure mechanism is similar to the postulated mechanism of Broms (1964) theory, while the depth of the second hinge (f) and the ultimate lateral resistance (H) are in close agreement with the solution of Barton (1982). The variability of the M_y of model piles is a plausible explanation for the differences in lateral resistance (for load path 3) between the heavily- and the lightly-loaded pile group (Fig. 18).

6. Non-destructive vibration tests

Realistic evaluation of the actual stiffness and capacity of pile groups is a prerequisite for rational retrofit design. Based on numerical analysis, Marin & Anastasopoulos (2021) recently proposed a simplified in-situ stiffness estimation method. The latter uses low-amplitude non-destructive dynamic loading to measure the lateral vibration response of the bridge-foundation system, obtaining stiffness estimates through simplified equations of motion. To experimentally investigate the efficiency of such a technique, a novel exploratory experimental setup is developed herein. To that end, the bridge–pilegroup model is subjected to cyclic low-amplitude non-destructive lateral loading and the generated vibrations are recorded. The tests performed explore the possibility to identify the natural period of structural systems founded on pile groups, and to estimate the small-strain rocking stiffness of the foundation.

As shown in Fig. 20, the experimental setup is based on the model of the lightly-loaded pile group. The key element of this setup is the dynamic piezoactuator used to apply cyclic low-amplitude non-destructive forces of given frequencies at the top of the model structure. The implemented system is similar to that of Cabrera et al. (2012) and Futai et al. (2018) with some adaptations, using the APA300ML dynamic actuator in conjunction with the LA75B

linear amplifier, both developed by Cedrat Technologies. The actuator is fully fixed to a load cell in a hosting frame at one end, while the other end is free to move on a linear bearing. The hosting frame is designed in such a way that the total mass (frame, load cell, actuator, and linear bearing) is identical to the concentrated mass used in the previous tests. Moreover, the actuator is installed at the centre of the concentrated mass of the static tests (i.e., 120 mm above the reference point).

The input excitation is recorded by a load cell attached between the actuator and the hosting frame. The response of the excited system is recorded by a set of piezoelectric accelerometers (one at actuator level and one close to the base of the superstructure) and capacitive displacement transducers (MicroEpsilon CapaNC DT CS05) with a measurement range of 0.5 mm and 10 nm resolution. The system is subjected to 50 cycles of force-controlled vibration loading with frequencies ranging from 1 Hz to 10 Hz (100 to 1000 Hz in model scale), increasing in steps of 1 Hz (100 Hz in model scale). Additionally, the system is excited at 8.5 Hz (850 Hz in model scale), which is the resonant frequency of the piezoactuator.

Figure 21 shows the dynamic measurements for two characteristic frequencies (1 Hz and 8.5 Hz). A zero-pole-gain low-pass Butterworth filter is used for post-processing, aiming to eliminate parasitic signals above the excitation frequency. Unfortunately, not all instruments functioned properly, as one of the capacitive displacement transducers was affected most probably by water drops from the in-flight saturation process, failing to record any data. All signals are much stronger for 8.5 Hz excitation frequency, where the actuator resonates (resulting in small residual deformations in this case).

Figure 22a summarizes the evaluation of the post-processed measurements in terms of maximum applied force for each excitation frequency. The maximum amplitude of dynamic force is reached at the resonance frequency of the piezoactuator (8.5 Hz) and exceeds the static lateral capacity of the system, observed in the pushover tests. Moving away from resonance frequency, the applied force drops swiftly for the frequency range of 1 Hz to 6 Hz.

The dynamic response of the model at each excitation frequency is evaluated as proposed by Futai et al. (2018), by normalizing the maximum accelerations measured at the top (or the maximum displacements in analogy) to the maximum applied force (Fig. 22b). The peak normalized response is observed at 1 Hz, where the generated displacements are comparable to the case of 8.5 Hz, despite the substantially lower applied force (two orders of magnitude

lower as shown in Fig. 21). This is an indication of the natural frequency of the examined system, which is expected to be around 1 Hz. More accurate identification of the natural frequency of the system would require more tests around this frequency, which were not possible as the laboratory had to close for refurbishment right after the tests were conducted. For excitation frequencies above 1 Hz (100 Hz in model scale), the response is de-amplified and the measurements become less suitable for the evaluation of dynamic response in terms of stiffness estimation, considering also the frequency dependency of stiffness and damping.

The measurements obtained at 1 Hz are used to evaluate the efficiency of the simplified methodology of Marin & Anastasopoulos (2021) for in-situ estimation of foundation rocking stiffness. For this purpose, the model is treated as a SDOF system. Simplifying assumptions are made regarding the mass participating in the rocking mode, which is assumed to include 30% of the pier, in addition to the concentrated mass (representing the bridge deck). The inertia force is calculated using the acceleration measurements, and subtracted from the force applied by the piezoactuator. The resultant force acting on the system is multiplied by the pier height to estimate the moment acting at the reference point. Due to the previously mentioned malfunctioning of one displacement transducer, the rotation (θ) is estimated using the available displacement measurements, and assuming the pole of rotation derived from the lateral pushover tests.

Based on these assumptions, the moment–rotation ($M - \theta$) loops of Fig. 22c are derived. The secant rocking stiffness derived from these loops is compared in Fig. 22d to the static pushover curve, revealing reasonable agreement. Overall, the developed non-destructive vibration testing experimental setup can be considered to offer promising results. However, only one test was successfully performed and the outcome of this study should be treated with prudence. In future tests with this setup, excitation frequencies closer to the expected natural frequency of the examined system should be investigated in more detail, since response de-amplification away from the natural frequency of the system can be substantial. Moreover, direct measurement of both accelerations and displacements was proven essential for realistic evaluation of dynamic response. Displacement estimations obtained by integration of acceleration measurements (or reciprocal) should be used with caution.

7. Summary and Conclusions

In the context of developing rational design methods for the retrofit of existing bridges on pile groups, this study has introduced a number of recent experimental developments at the ETHZ Drum centrifuge. Using only part of the channel's circumference, thus operating the drum similar to a beam centrifuge, four different experimental setups were presented: (1) vertical loading; (2) lateral pushover loading; (3) combined (*VHM*) loading; and (4) non-destructive vibration testing. The implemented experimental procedures were successfully evaluated in producing controlled and repeatable test results, and their capabilities and limitations were illustrated, using a prototype problem of a 2 x 1 bored pile group on saturated dense sand.

Starting with the vertical loading of single piles and pile groups, the important role of installation method and pile roughness was explored and quantified. Four different installation methods were investigated: (i) monotonic jacking at 1g (bored piles); (ii) monotonic jacking at 100g (jacked piles, simplified); (iii) load-controlled cyclic jacking at 100 g (jacked piles); and (iv) displacement-controlled cyclic jacking at 100g (driven piles). The results were used to highlight the uncertainties and the poor predictive capability of traditional bearing capacity approaches. The unavoidable shortcomings of centrifuge model testing related to scale effects on the shaft resistance mechanism were also critically discussed.

Pushover loading was employed to measure the moment capacity (M_{ult}) of a lightly-loaded ($FS_v = 3$), and a heavily-loaded ($FS_v = 1.5$) 2 x 1 bored pile group, representing the existing and the widened bridge (without any foundation retrofit), respectively. In contrast to what would be intuitively expected, the heavily-loaded system was found to mobilise significantly higher M_{ult} . The mechanism leading to the increase of M_{ult} with decreasing FS_v was partially explained using the measured response of single piles subjected to vertical loading. Despite playing a key role, the axial pile loading mechanism cannot fully explain the observed response, as it underestimates the measured M_{ult} by up to 50%. The contribution of the cap and the additional mobilised resistance due to lateral loading of the piles was shown to be non-negligible. The latter is more pronounced in the centrifuge tests due to the overestimation of the bending moment capacity (M_y) of the model piles.

A combined (*VHM*) loading apparatus was developed, consisting of two actuators mounted on the strong-box, combined with the 2DOF actuator of the tool platform. The actuators are connected through a mechanical assembly, consisting of rigid aluminium parts and two hinges. The developed experimental setup was proof tested for a shallow square foundation. The results were compared to published failure envelopes, achieving satisfactory agreement. A simplified version of this assembly was then implemented to subject the studied pile group to combined loading under constant vertical load. Experimental failure envelopes were derived, revealing significant coupling between lateral (H) and moment (M) loading, and confirming the expansion of the failure envelope with increasing vertical load. The failure modes were analysed and two mechanisms were identified (single or double hinged), depending on whether H or M is dominant. Single fixed-head piles were also tested and compared to the Limit Equilibrium solution of Barton (1982), showing good agreement.

Finally, an exploratory study on non-destructive vibration testing of existing pile groups was attempted. The developed experimental setup uses a dynamic piezoactuator to apply cyclic low-amplitude non-destructive forces of given frequencies at the top of the model structure. The actuator is fully fixed to a load cell in a hosting frame at one end, while the other end is free to move on a linear bearing. The developed setup was proof-tested for the lightly-loaded ($FS_v = 3$) pile group, imposing vibration signals of varying frequencies. The results are promising, confirming the possibility to identify the natural frequency of the system and the small-strain stiffness of the foundation through non-destructive vibration testing.

Although this study was fuelled by our ongoing work on pile groups, the developed experimental setups are of general applicability for the study of deep and shallow foundation systems.

Acknowledgement

Financial support for this work has been provided by the Swiss Federal Roads Office (FEDRO) within the project AGB2017/001 (“Development of reliable methods for optimized retrofit design of bridge pile groups”) and is gratefully acknowledged. The authors would also like to acknowledge the contribution of Floriane Bühler, Séverin Perrey, Max Sieber and Nicole Schwerzmann for the soil element tests presented in the paper, and Andrea Ciancimino and Jürg Giger for their support and suggestions for the conducted centrifuge experiments.

Nomenclature

The following symbols are used in this paper:

| | |
|-----------------|--|
| a | acceleration time history |
| B | foundation / pile cap width |
| C_u | uniformity coefficient |
| D | pile diameter |
| D_r | relative density |
| D_{10} | 10% pass particle size |
| D_{50} | 50% pass particle size |
| e_{vol} | volumetric strain |
| e_{min} | minimum void ratio |
| e_{max} | maximum void ratio |
| FS_v | safety factor under vertical loading |
| F | force (3 point bending/cantilever tests) |
| f | depth of plastic hinge |
| H | horizontal force |
| H_o | maximum horizontal force (swipe tests) |
| h | pier height |
| K | lateral earth pressure coefficient |
| K_p | passive earth pressure coefficient |
| K_r | rocking stiffness |
| L | pile length |
| M | overturning moment |
| M_{ult} | pile group moment capacity |
| M_y | piles' bending moment capacity |
| N_q | bearing capacity factor |
| p_o' | confining stress |
| q | deviatoric stress |
| s | pile spacing |
| t | thickness of hollow aluminium section |
| u | lateral displacement |
| V | vertical force |
| V_o | maximum vertical force (swipe tests) |
| V_{tip} | tip resistance |
| V_{shaft} | shaft resistance |
| w | settlement |
| δ' | Interface friction angle |
| δ | lateral displacement (atop) |
| δ_{base} | lateral displacement (base) |
| ε | axial strain |

| | |
|-------------------------------------|---|
| θ | rotation |
| σ | axial Stress |
| σ'_v | Vertical effective stress |
| τ | shear stress |
| ρ_d | dry density |
| φ'_{peak} | peak friction angle ($^\circ$) |
| φ'_{cv} | constant volume friction angle ($^\circ$) |
| <u>Combined Loading Apparatus</u> | |
| l_i, r_i | setup parameters (initial position) |
| $\delta L_i, \delta x_{tp}$ | actuator movement (incremental) |
| $\delta x, \delta y, \delta \theta$ | target displacement path (incremental) |

References

- Arnold, A. (2011). *Tragverhalten von nicht starren Flachfundamenten unter Berücksichtigung der lokalen Steifigkeitsverhältnisse* (No. 19516).
- Anastasopoulos, I., Kourkoulis, R., Gelagoti, F., & Papadopoulos, E. (2012). Rocking response of SDOF systems on shallow improved sand: An experimental study. *Soil Dynamics and Earthquake Engineering*, 40, 15-33.
- Barton, Y.O. (1982). *Laterally loaded model piles in sand: Centrifuge tests and finite element analyses*, Doctoral dissertation, University of Cambridge.
- Berezantsev, V.G. (1961). Load bearing capacity and deformation of piled foundations. In *Proc. of the 5th International Conference, ISSMFE, Paris, 1961* (Vol. 2, pp. 11-12).
- Bolton, M.D. (1986). The strength and dilatancy of sands. *Geotechnique*, 36(1), 65-78.
- Bolton, M.D., Gui, M.W., Garnier, J., Corte, J. F., Bagge, G., Laue, J., & Renzi, R. (1999). Centrifuge cone penetration tests in sand. *Géotechnique*, 49(4), 543-552.
- Borghi, X., White, D. J., Bolton, M. D., Springman, S. (2001). Empirical pile design based on cone penetrometer data: an explanation for the reduction of unit base resistance between CPTs and piles. *5th Int. Conf. on Deep Found. Practice, Singapore*, 125-132.
- Broms, B. B. (1964). Lateral resistance of piles in cohesionless soils. *Journal of the soil mechanics and foundations division*, 90(3), 123-156.
- Burali D'Arezzo, F., Haigh, S. K., Ishihara, Y., Gaudin, C., & White, D. (2014). Modelling of jacked piles in centrifuge. In *8th Intern. Conf. on Physical Modelling in Geotechnics, Perth, Australia*.
- Cheng, N., & Cassidy, M. J. (2016). Combined loading capacity of spudcan footings on loose sand. *International Journal of Physical Modelling in Geotechnics*, 16(1), 31-44.
- Dean, E. T. R., James, R. G., Schofield, A. N., & Tsukamoto, Y. (1997). Theoretical modelling of spudcan behaviour under combined load. *Soils and foundations*, 37(2), 1-15.
- De Nicola, A., & Randolph, M. F. (1997). The plugging behaviour of driven and jacked piles in sand. *Geotechnique*, 47(4), 841-856.





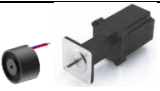





- De Nicola, A., & Randolph, M. F. (1994). Development of a miniature pile driving actuator. In *International conference centrifuge 94* (pp. 473-478).
- Di Laora, R., L. de Sanctis, S. Aversa. (2019). Bearing capacity of pile groups under vertical eccentric load. *Acta Geotech.* 14 (1): 193–205.
- Fellenius, B. H. (1999). Bearing capacity of footings and piles—A delusion. In *Proceedings of the Deep Foundation Institute Annual Meeting, October* (Vol. 14, p. 17).FEMA.
2009. Recommended seismic provisions for new buildings and other structures. FEMA 750. Washington, DC: Building Seismic Safety Council, National Institute of Building.
- Fioravante, V. (2002). On the shaft friction modelling of non-displacement piles in sand. *Soils and foundations*, 42(2), 23-33.
- Fleming, K., Weltman, A., Randolph, M., & Elson, K. (2008). *Piling engineering*. CRC press.
- Gajan, S., Kutter, B. L., Phalen, J. D., Hutchinson, T. C., & Martin, G. R. (2005). Centrifuge modeling of load-deformation behavior of rocking shallow foundations. *Soil Dynamics and Earthquake Engineering*, 25(7-10), 773-783.
- Gan, C. T., Leung, C. F., Cassidy, M. J., Gaudin, C., & Chow, Y. K. (2012). Effect of time on spudcan–footprint interaction in clay. *Géotechnique*, 62(5), 401-413.
- Gottardi, G., Houlsby, G. T., & Butterfield, R. (1999). Plastic response of circular footings on sand under general planar loading. *Géotechnique*, 49(4), 453-469.
- Gue, C. S., Soga, K., Bolton, M., & Thusyanthan, N. I. (2010). Centrifuge modelling of submarine landslide flows. *Stress*, 2(2), 8.
- El Haffar, I., Blanc, M., & Thorel, L. (2017). Impact of pile installation method on the axial capacity in sand. *Géotechnique Letters*, 7(3), 260-265.
- Futai, M. M., Dong, J., Haigh, S. K., & Madabhushi, S. G. (2018). Dynamic response of monopiles in sand using centrifuge modelling. *Soil Dynamics and Earthquake Engineering*, 115, 90-103.
- Ismael, N. F. (1989). Field tests on bored piles subject to axial and oblique pull. *Journal of Geotechnical Engineering*, 115(11), 1588-1598.
- Knappett, J. A., Reid, C., Kinmond, S., & O'Reilly, K. (2011). Small-scale modeling of reinforced concrete structural elements for use in a geotechnical centrifuge. *Journal of Structural Engineering*, 137(11), 1263-1271.
- Laue, J., Nater, P., Springman, S. M. (2002). Preparation of soil samples in drum centrifuges. *International Conference on Physical Modelling in Geotechnics/ICPGM'02, St. John's, New Foundland, Canada, 10-12 July 2002* (pp. 143-148). Balkema.
- Lehane, B. M., & White, D. J. (2005). Lateral stress changes and shaft friction for model displacement piles in sand. *Canadian geotechnical journal*, 42(4), 1039-1052.
- Lehane, B. M., Gaudin, C., & Schneider, J. A. (2005). Scale effects on tension capacity for rough piles buried in dense sand. *Géotechnique*, 55(10), 709-719.
- Loli, M., Knappett, J.A., Brown, M.J., Anastasopoulos, I., Gazetas, G. (2014), “Centrifuge modeling of rocking–isolated inelastic RC bridge piers”, *Earthquake Engineering and Structural Dynamics*, 43(15): 2341–2359.

- Loukidis, D., & Salgado, R. (2008). Analysis of the shaft resistance of non-displacement piles in sand. *Géotechnique*, 58(4), 283-296.
- Madabhushi, Gopal. *Centrifuge modelling for civil engineers*. CRC Press, 2014.
- Marin, A., & Anastasopoulos, I. (2021). Existing bridges on pile groups: In-situ measurement of stiffness. *Soil Dynamics and Earthquake Engineering*, 148, 106797.
- Martin CM (1994) Physical and Numerical Modelling of Offshore Foundations under Combined Loads. DPhil thesis, University of Oxford, Oxford, UK.
- Miyamoto, J., Miyake, M., Tsurugasaki, K., Sumida, H., Sawada, Y., Maeda, K., & Matsuda, T. (2015, July). Instability of breakwater foundation during tsunami in a drum centrifuge. In *The Twenty-fifth International Ocean and Polar Engineering Conference*. International Society of Offshore and Polar Engineers.
- Morales, W. F., Laue, J., Springman, S. M. (2013). On the use of unsaturated properties of a sandy material for centrifuge model preparation. *Advances in Unsat. Soils*, 1, 159.
- National Instruments Corporation (2003) LabVIEW User Manual. NIC, Austin, TX, USA.
- Poulos, H. G. (2017). *Tall building foundation design*. CRC Press.
- Springman, S., Laue, J., Boyle, R., White, J., Zweidler, A. (2001). The ETH Zurich geotechnical drum centrifuge. *Inter. Journal of Physical Modelling in Geotechnics*, 1(1), 59-70.
- Taeseri, D., Laue, J., Martakis, P., Chatzi, E., & Anastasopoulos, I. (2018). Static and dynamic rocking stiffness of shallow footings on sand: centrifuge modelling. *International Journal of Physical Modelling in Geotechnics*, 18(6), 315-339.
- Tan, F. S. C. (1990). Centrifuge and theoretical modelling of conical footings on sand. PhD thesis, University of Cambridge.
- Terzaghi, K. (1943). Theoretical soil mechanics, chapter 8. New York: Wiley.
- Ticof, J. (1977). Surface footings on sand under general planar loads. PhD thesis, Southampton University.
- Viggiani, C., Mandolini, A., & Russo, G. (2014). *Piles and pile foundations*. CRC Press.
- Yin, M., Rui, Y., & Xue, Y. (2019). Centrifuge study on the runout distance of submarine debris flows. *Marine Georesources & Geotechnology*, 37(3), 301-311.
- Zhang, Y., Bienen, B., & Cassidy, M. J. (2013). Development of a combined VHM loading apparatus for a geotechnical drum centrifuge. *International Journal of Physical Modelling in Geotechnics*, 13(1), 13-30.
- Zhao, R., Leung, A. K., Knappett, J., Robinson, S., & Brennan, A. (2021). Nonlinear Lateral Response of RC Pile in Sand: Centrifuge and Numerical Modelling. *Journal of Geotechnical and Geoenvironmental Engineering*, 147(6), 04021031.

Table 1. Active drum centrifuge facilities around the world.

| Institute, Location | Diameter |
|--|----------|
| University of Cambridge, UK | 1.2 m |
| University of West Australia, Australia | 1.2 m |
| Tokyo Institute of Technology, Japan | 1.2 m |
| Kiso-jiban Consultants Co., Japan | 1.2 m |
| University of Texas at Austin, USA | 1.4 m |
| Dalian University of Technology, PR China | 1.4 m |
| Toyo Construction Co., Japan | 2.2 m |
| Western Geotechnical Research Centre, Canada | 2.2 m |
| ETH Zurich, Switzerland | 2.2 m |

Table 2. Implemented devices and instruments for the four test series.

| Instrument | Type | Specifications | |
|---------------------------------|---|------------------------------------|---|
| solenoid valves | ASCO (SCG238A044) | 0 -10bar |  |
| pumps | Ismatec ism895e | 1 – 3290 ml/min |  |
| pore pressure transducers (PPT) | Druck | 7 bar |  |
| actuators* | Progressive automations PA-09 | 1.48kN |  |
| support actuator/ magnet | Nanotec Stepper Motor ST5918 Isliker Magnete GT-40 | 0.4 kN |  |
| load cells | MTS Burster 8435 | 2 kN |  |
| lasers | Micro-Epsilon optoNCDT 1420 | 100 – 200 mm |  |
| accelerometers | Brüel&Kjaer Type 4374 | 1 - 26000Hz 25000g |  |
| piezoelectric actuator | Cedrat APA300ML | 250N at 850Hz |  |
| capacitive sensor | Micro-Epsilon CapaNCDT CS05 | Range: 0.5 mm Resolution: 10 nm |  |

*Customised in-house, replacing the original Brushed DC Motor with Stepper Motor Phytron ZSS 32.200, for enhanced precision at high g-levels

Table 3. Soil parameters of Perth Sand

| parameter | value | description |
|----------------|-------|-----------------------------------|
| USCS | SP | classification |
| D_{10} | 0.14 | effective particle size (mm) |
| D_{50} | 0.22 | average particle size (mm) |
| C_u | 1.79 | uniformity coefficient |
| D_r | 80 | relative density (%) |
| ρ_d | 1720 | dry density (kg/m ³) |
| e_{min} | 0.44 | minumum void ratio |
| e_{max} | 0.81 | maximum void ratio |
| ϕ'_{cv} | 29.6 | critical state friction angle (°) |
| ϕ'_{peak} | 42 | peak friction angle (°) |

Table 4. Overview of the conducted vertical loading tests (Phase A).

| Test ID | Installation method | Prototype conditions | Interface | Layout |
|---------|---------------------|----------------------|---------------|-------------------------|
| LSA1i | 1g-MJ | Bored | <i>smooth</i> | <i>single pile</i> |
| LSA1ii | 100g-MJ | Jacked | | |
| LSA1iii | 100g-CJ-DC | Driven | | |
| LSA2i * | 1g-MJ | Bored | | |
| LSA2ii* | 100g-MJ | Jacked | | |
| LSA2iii | 100g-CJ-LC | Jacked | | |
| LSA3i | 1g-MJ | Bored | <i>rough</i> | <i>single pile</i> |
| LSA3ii | 100g-MJ | Jacked | | |
| LSA3iii | 100g-CJ-DC | Driven | | |
| LSA4i * | 1g-MJ | Bored | | |
| LSA4ii* | 100g-MJ | Jacked | | |
| LSA4ii | 100g-CJ-LC | Jacked | | |
| LSA5 | 1g-MJ | Bored | <i>rough</i> | <i>group, s/D=3</i> |
| LSA6 | | | | <i>group, s/D=4</i> |
| LSA7 | | | | <i>group, s/D=2</i> |
| LSA8 | | | | <i>group s/D=3 / w/</i> |

*Repeatability assessment

Table 5. The effect of installation method and pile roughness on single pile vertical bearing capacity and pull-out resistance.

| Installation method | Prototype conditions | Bearing capacity* (MN) | | Pull out resistance (MN) | |
|--|----------------------|------------------------|--------------|--------------------------|--------------|
| | | <i>Smooth</i> | <i>Rough</i> | <i>Smooth</i> | <i>Rough</i> |
| MJ – 1 g | Bored | 4.8 | 7.9 | -1.2 | -1.9 |
| MJ – 100 g | Jacked | 27.9 | 35.0 | -3.9 | -3.9 |
| DC – 100 g | Driven | 31.0 | 37.4 | -4.0 | -7.2 |
| LC – 100 g | Jacked | 31.6 | 45.6 | -5.7 | -6.7 |
| * Bearing capacity is determined as the load at settlement $w/D = 0.1$ | | | | | |

Table 6. Overview and details of centrifuge tests of phases B, C, D

| Test ID | Type of loading | Details |
|---------|--|---|
| LSB1 | <i>pushover</i> | $FS_v = 3.0$ |
| LSB2* | | |
| LSB3 | | $FS_v = 1.5$ |
| LSCi | <i>combined under constant vertical displacement (swipe)</i> | swipe u ($\theta=0$) |
| LSCii | | swipe u ($\theta=0$) w/o sidewalls |
| LSC1 | <i>combined under constant vertical load</i> | $FS_v = 3.0, u$ ($\theta = 0$) |
| LSC2 | | $FS_v = 1.5, u$ ($\theta = 0$) |
| LSC3 | | $FS_v = 3.0, \theta$ ($u = 0$) |
| LSC4 | | $FS_v = 1.5, \theta$ ($u = 0$) |
| LSC5 | | $FS_v = 3, u$ ($\theta = 0$) out of plane |
| LSD1 | <i>vibration</i> | $FS_v = 3$ |

*Repeatability assessment

Figure captions

Fig. 1. Simplified prototype problem and experimental campaign overview.

Fig. 2. Plan view of the ETH Drum Centrifuge facility (top), along with cross section and plan view of the 2.2 m diameter Broadbent drum centrifuge (bottom) (based on Springman et al., 2001).

Fig. 3. Model preparation: (a) air pluviation overview: soil density in function of drop height h and diffuser opening d , and post-testing measured D_r ; and (b) Perth sand characterisation: CID triaxial tests expressed in normalised deviatoric stress (continuous lines) and volumetric strain (dashed lines) plotted against axial strain curves and CNL interface test at the target density and different confining stresses.

Fig. 4. Stages of model preparation: (a) dry sand pluviation outside the centrifuge; (b) controlled soil saturation; (c) de-saturation, development of matric suction; (d) transportation of the strong boxes; (e) installation in the drum channel and spin-up to 20g; and (f) controlled re-saturation at 20g.

Fig. 5. Comparisons of load-settlement behaviour between dry and partially saturated soil conditions for: (a) shallow foundation (Arnold, 2005); and (b) single smooth pile jacked monotonically at 100 g; (c) layout of the developed and implemented in-flight saturation system.

- Fig. 6. Vertical loading tests: (a) overview of the experimental setup; (b) linear slider (side view) to accommodate differential displacements during spin-up; and (c) instrumented pile tip (all dimensions in model scale).
- Fig. 7. Effects of installation method on the bearing capacity and pull out resistance of single piles. Vertical load–settlement response, where the settlement is normalized to the pile length (w/L) when considering the entire experiment, and the pile diameter (w/D) when focusing on the loading after installation: (a) smooth interface; and (b) rough interface.
- Fig. 8. Repeatability assessment and comparison to bearing capacity theory. Bearing capacity (compared to Fleming et al. 2008 and Berenzansev 1961) and pull out resistance (compared to the beta method, shaded area) of single rough pile jacked monotonically at: (a) 1g (bored piles); and (b) 100g (jacked piles). Post-test micro-scanning showing grain crushing during 100g installation.
- Fig. 9. The effect of pile roughness. Total, tip and shaft resistance in function of normalized settlement w/D for single piles installed at 1g (left) and at 100g (right): (a) smooth; and (b) rough interface.
- Fig. 10. Vertical loading of 2 x 1 pile group: (a) the effect of pile spacing s/D in the push-down (left) and pull-out (right) force–settlement ($V - w/D$) response; and (b) comparison of push-down and pull-out response of single piles to the pile group, with and without the contribution of the pile cap.
- Fig. 11. Model piles: (a) three-point bending tests of aluminium model piles with and without epoxy-sand coating; and (b) verification of model piles against section analysis of the prototype RC pile for the range of pile axial forces expected to develop during moment loading.
- Fig. 12. Illustration and photo (after spin down) of the experimental setup for the lateral pushover tests.
- Fig. 13. Lateral pushover test results for the lightly-loaded ($FS_v = 3$) and the heavily-loaded ($FS_v = 1.5$) pile group, in terms of: (a) force–displacement ($F - \delta$) response; (b) moment–rotation ($M - \theta$) response; (c) $M - \theta$ removing second order effects; (d) time history of displacement δ atop; and (e) displacement δ_{base} at the reference point; and (f) settlement–rotation ($w - \theta$) response.
- Fig. 14. Calculation of pile group moment–rotation ($M - \theta$) response on the basis of experimentally measured axial load–settlement ($V - w$) response for the lightly-loaded ($FS_v = 3$) and the heavily-loaded ($FS_v = 1.5$) pile group: (a) expected axial load path for the leading and the trailing piles; and (b) calculated vs. measured $M - \theta$ response.
- Fig. 15. Combined VHM loading: (a) illustration of application of purely vertical, horizontal, and rotational movement; (b) overview of the experimental setup for swipe testing and key geometrical quantities; and (c) photos of the experimental setup before testing.

Fig. 16. Proof testing of combined (MHV) loading experimental setup using a shallow foundation, also exploring the effect of the sidewalls: (a) first stage vertical loading; (b) normalized horizontal loading –displacement (H/V_o) response; (c) load paths in normalized $M - H$ space; and (d) normalized $H - V$ load path compared to the parabolic failure proposed by Gottardi et al. (1999).

Fig. 17. Illustration and overview of the constant vertical load test experimental setup.

Fig. 18. Constant vertical load tests. Load paths with ultimate load points and illustration of failure envelope in the $M - H$ space, and post-testing deformed models: (a) lightly-loaded ($FS_v = 3$); and (b) heavily-loaded ($FS_v = 1.5$) pile group. (1) Primarily moment loading ($u = 0$); (2) Pushover; and (3) primarily lateral loading ($\theta = 0$).

Fig. 19. Equivalent single pile subjected to lateral loading ($\theta = 0$): centrifuge model test results compared to the theory Broms (1964), considering fixed head conditions.

Fig. 20. Experimental setup for non-destructive vibration testing, comprising a piezo-actuator equipped with a load cell, pairs of accelerometers and capacitive displacement transducers.

Fig. 21. Non-destructive vibration testing: time histories of force, acceleration (top and base), and displacement for excitation frequencies of 1Hz and 8.5Hz.

Fig. 22. Evaluation of vibration testing: (a) force (F) in function of frequency (f); (b) acceleration (a) and displacement (δ) normalised to F ; (c) moment-rotation ($M - \theta$) loops of forced vibration at $f = 1\text{Hz}$, and estimation of rocking stiffness; and (d) comparison to pushover test results.

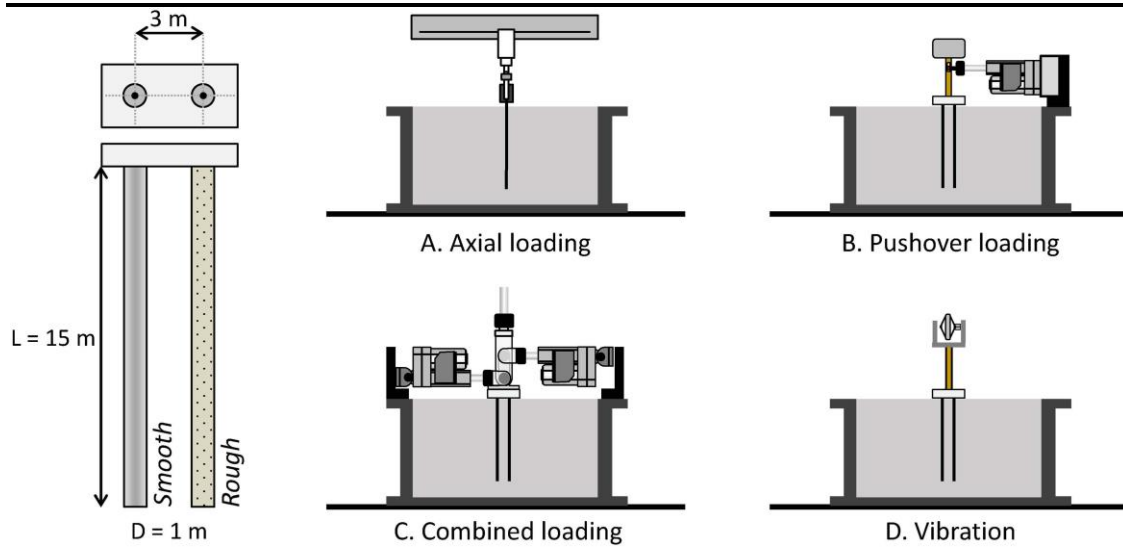


Fig. 1

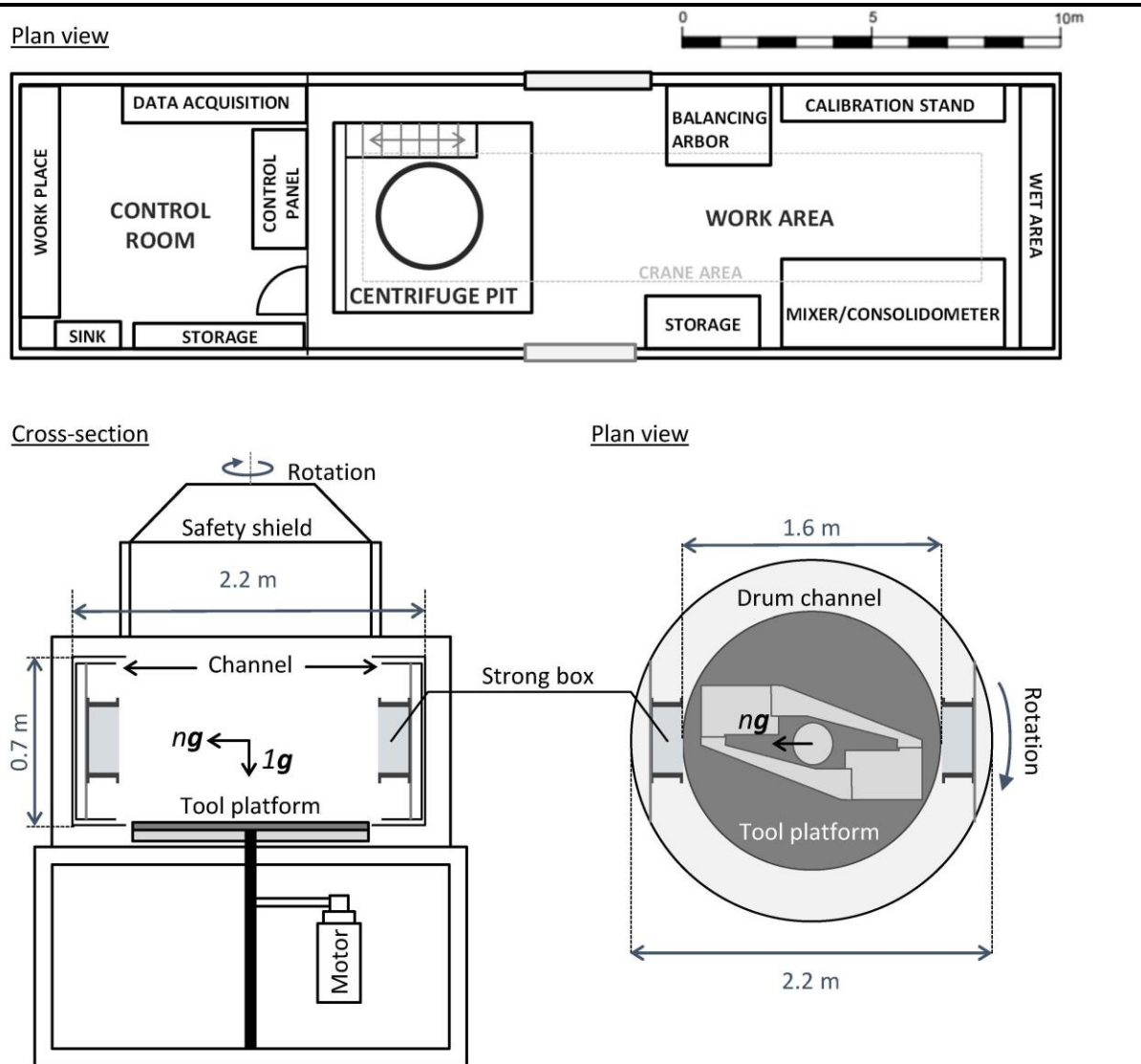


Fig. 2

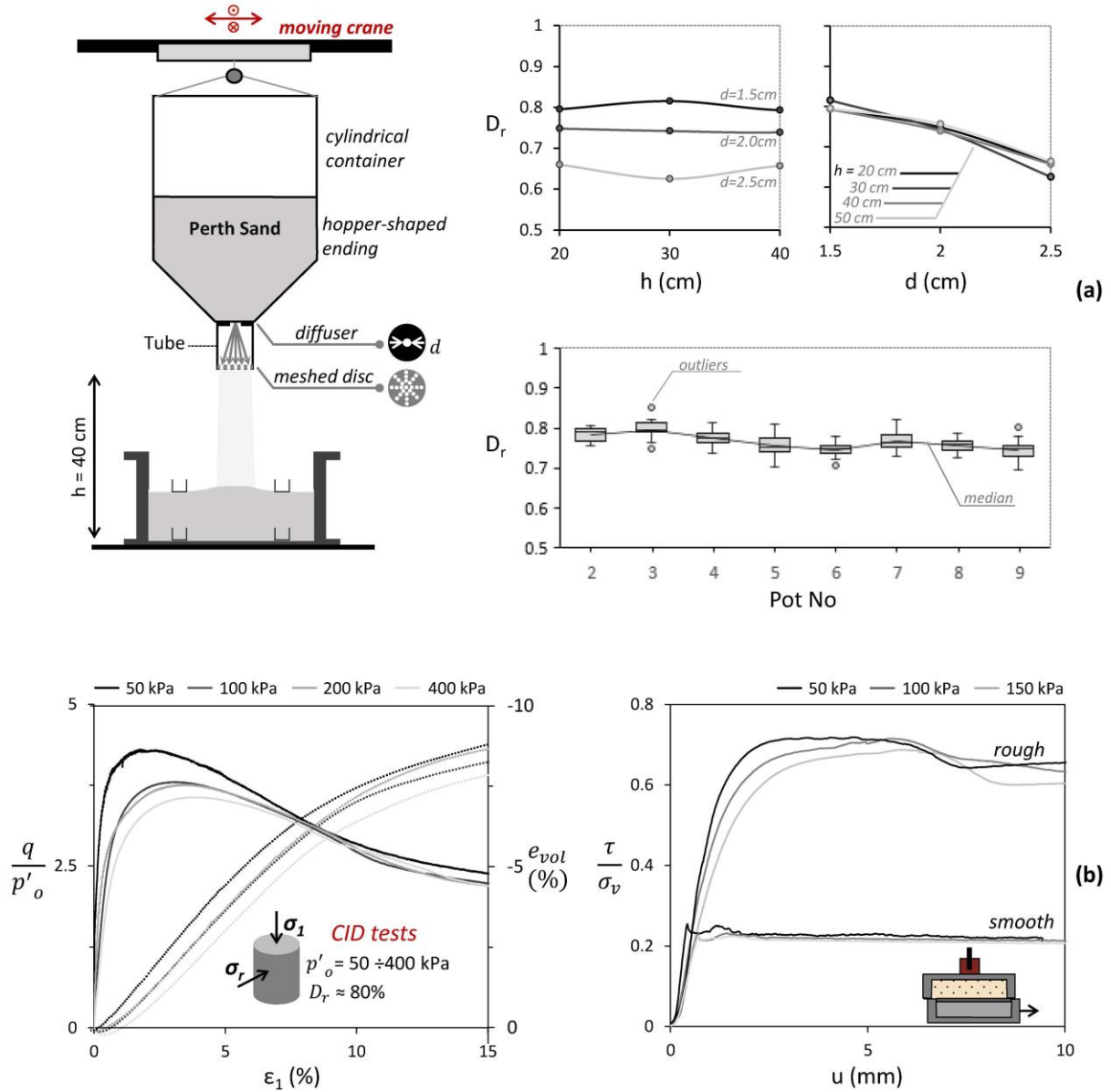


Fig. 3

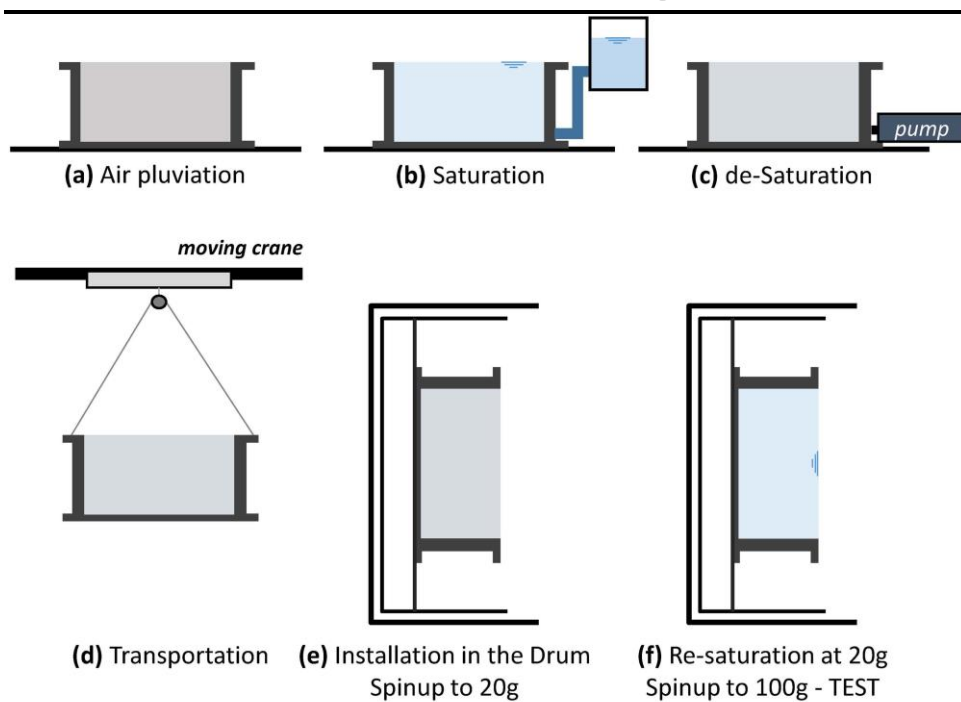


Fig. 4

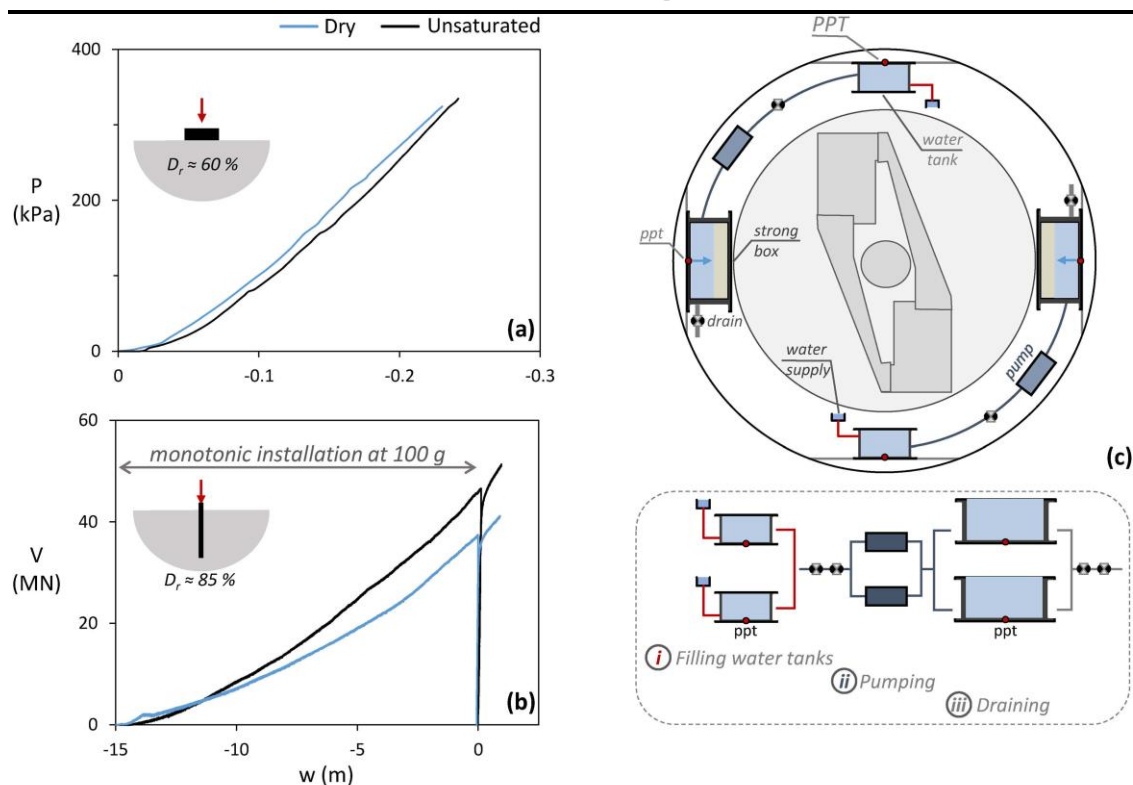


Fig. 5

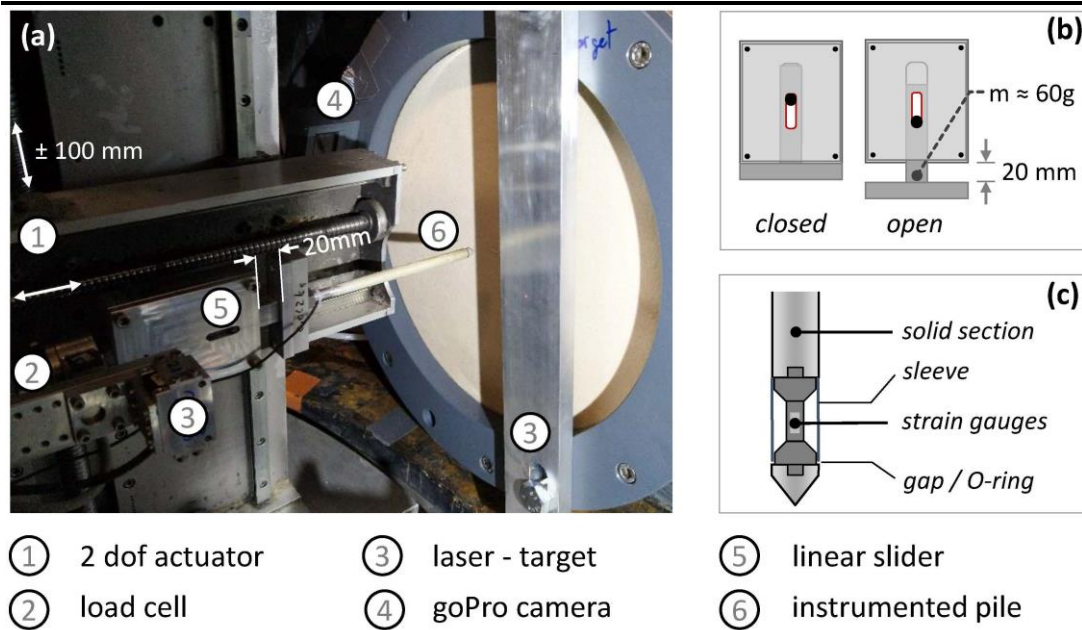


Fig. 6

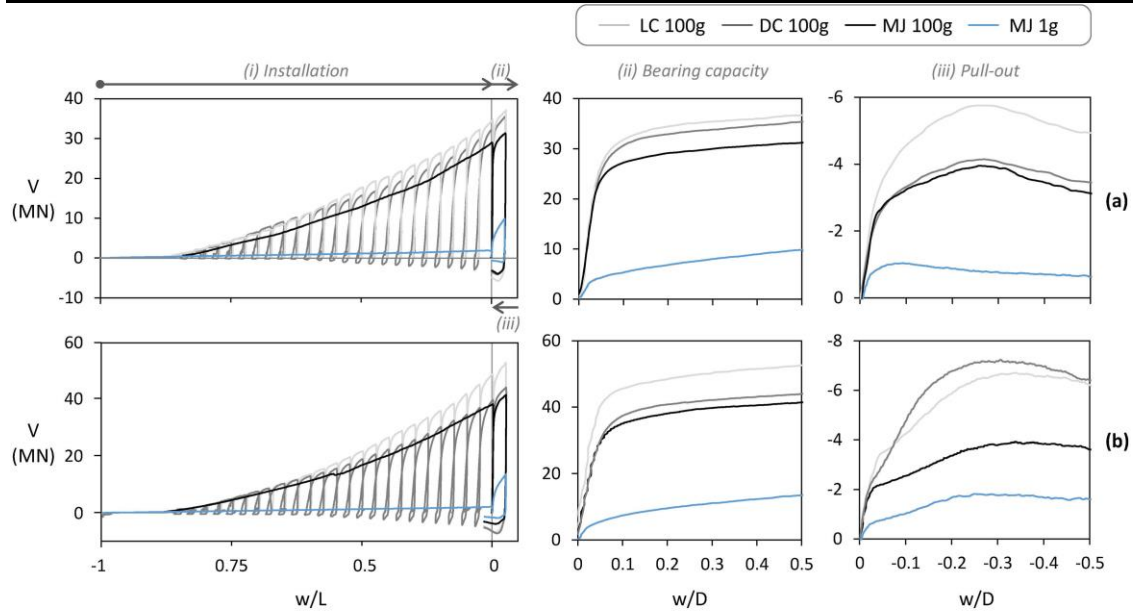


Fig. 7

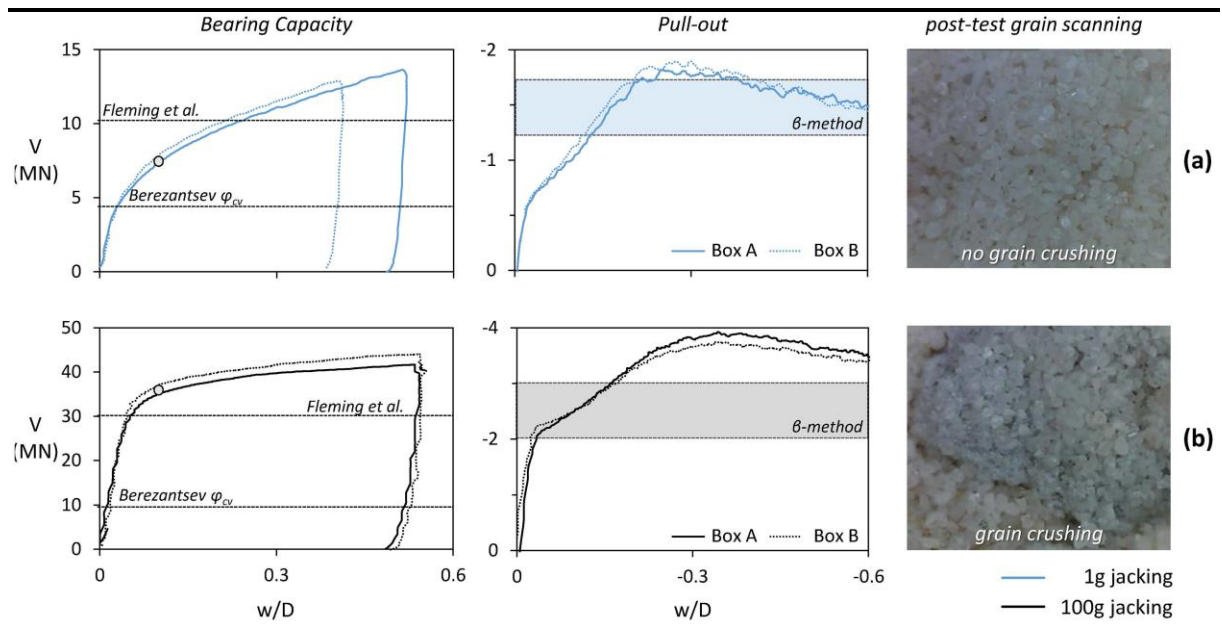


Fig. 8

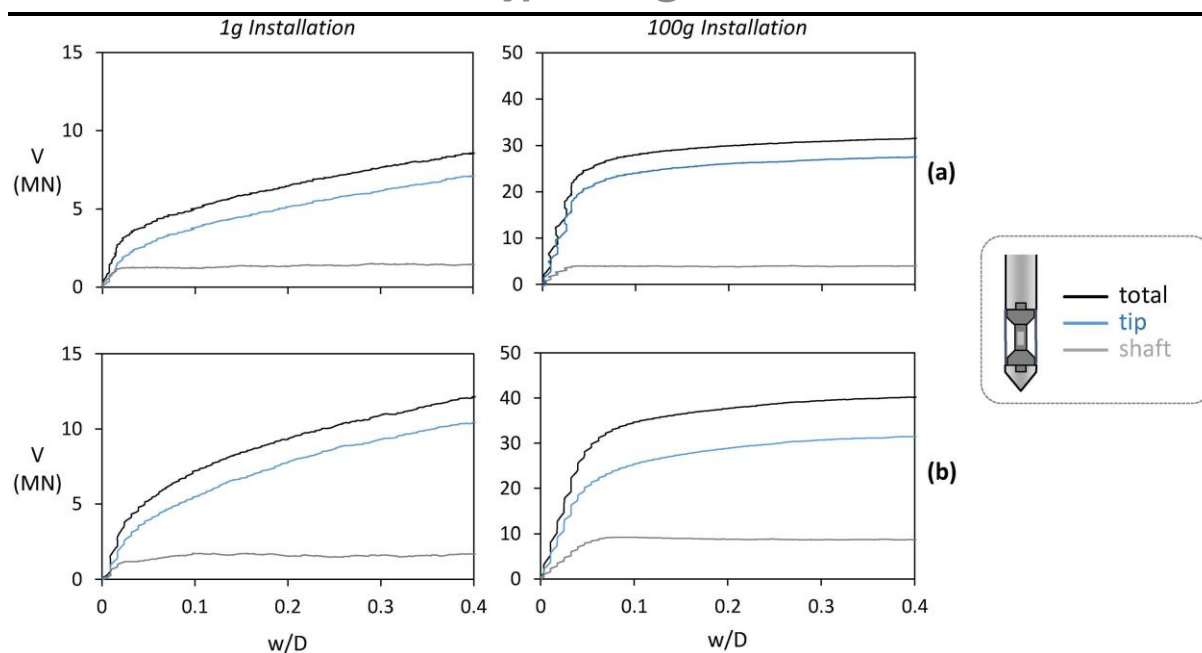


Fig. 9

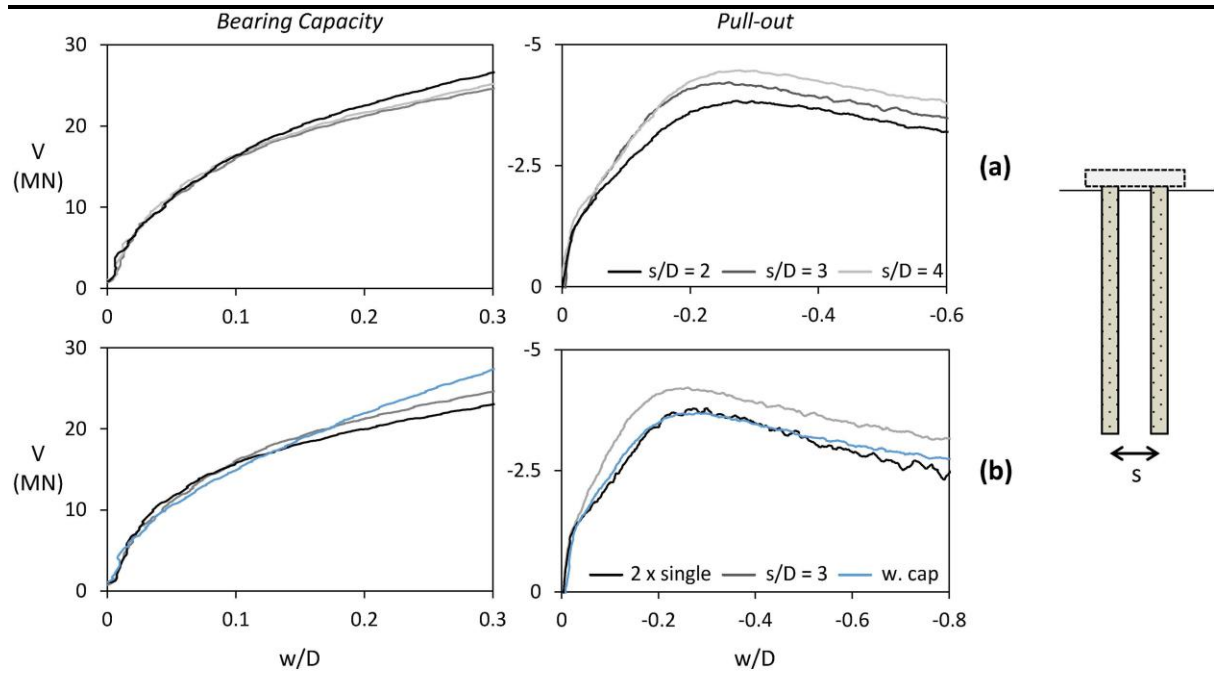


Fig. 10

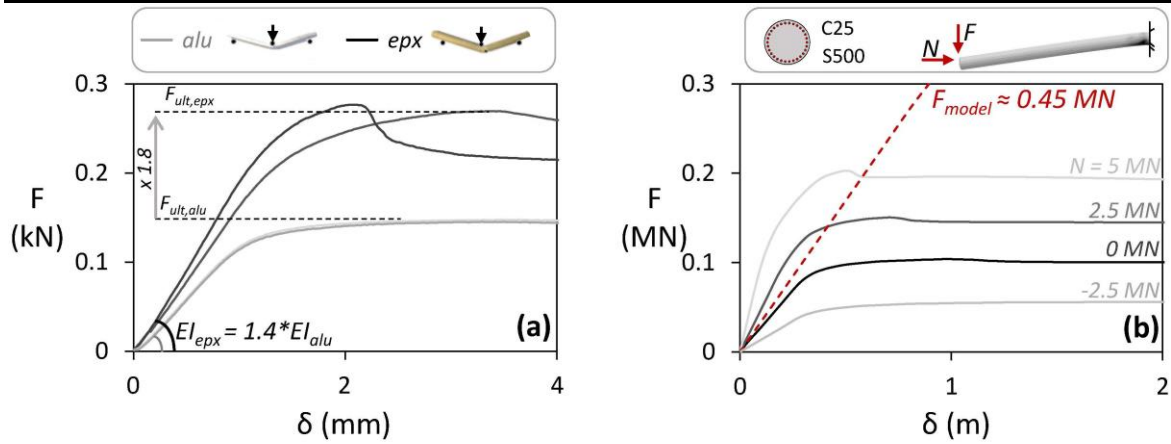


Fig. 11

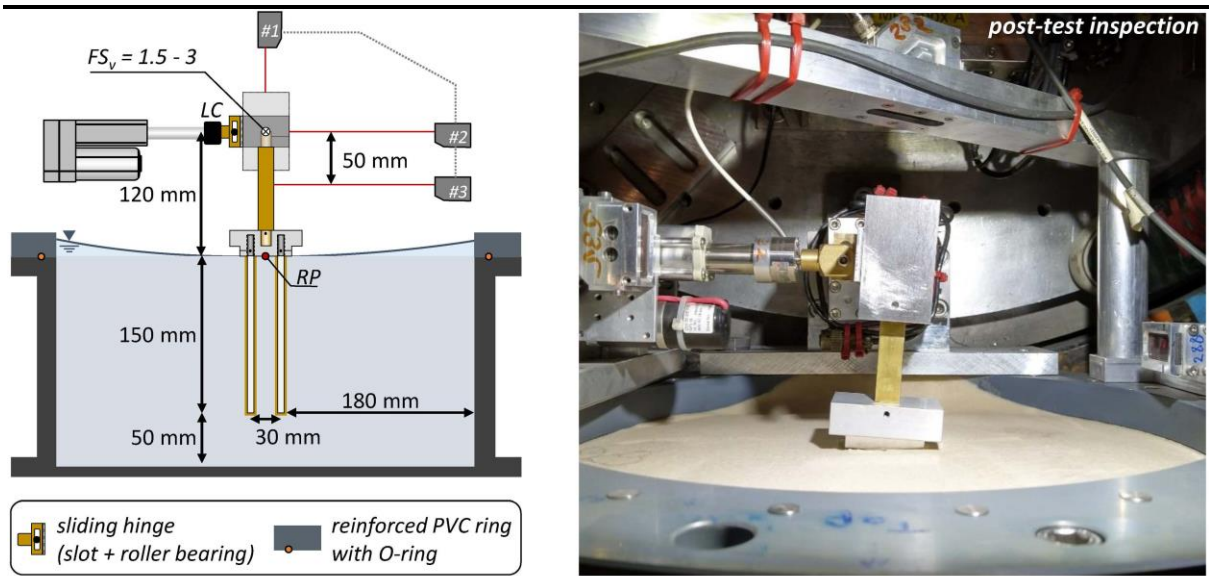


Fig. 12

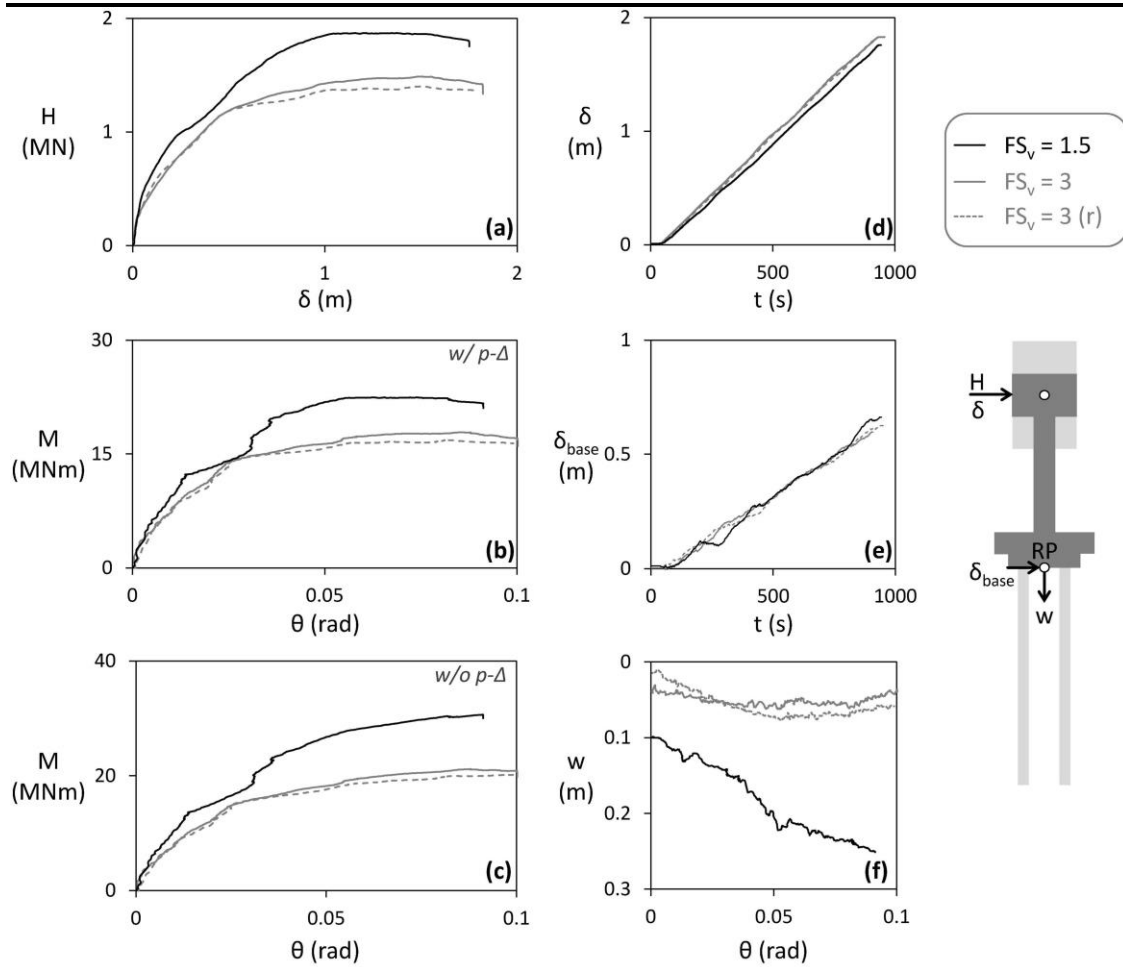


Fig. 13

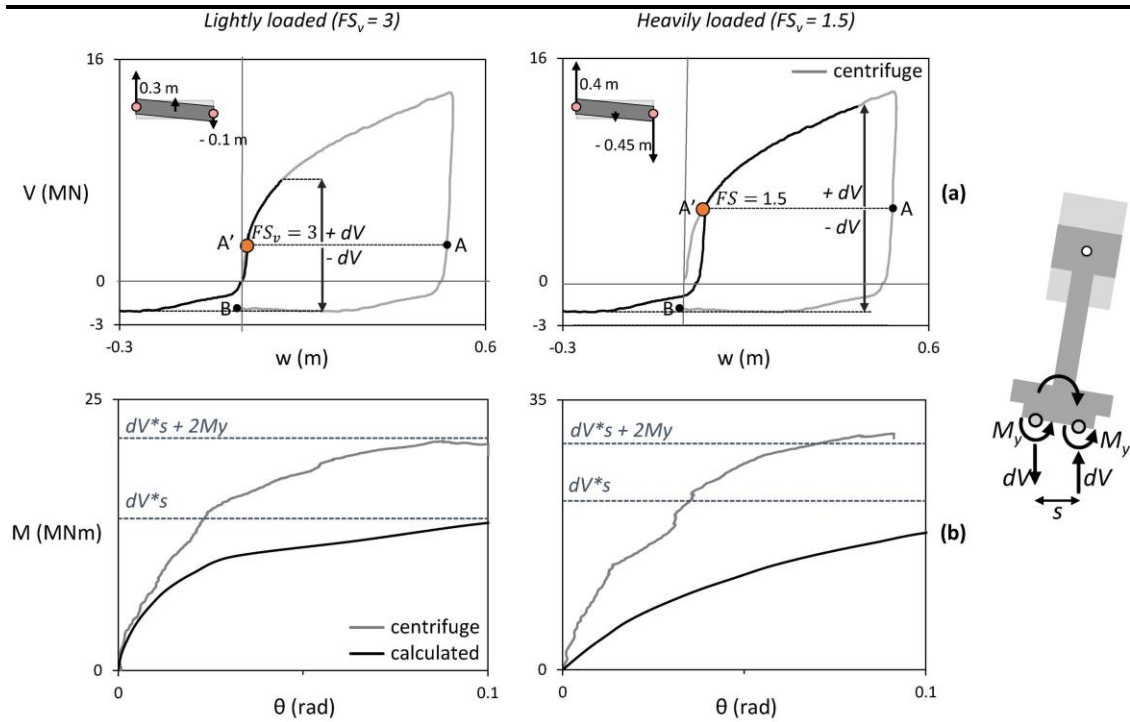


Fig. 14

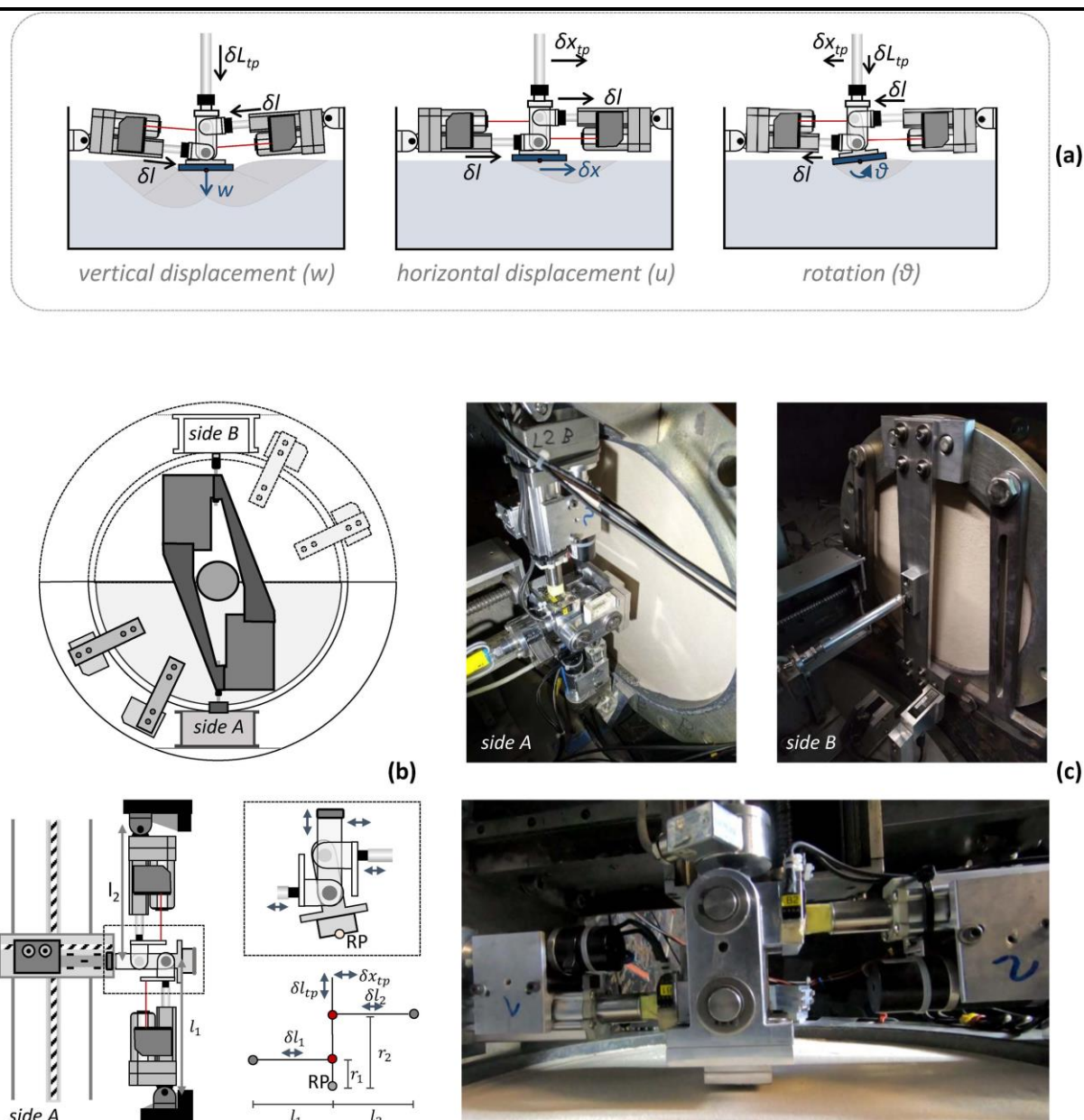


Fig. 15

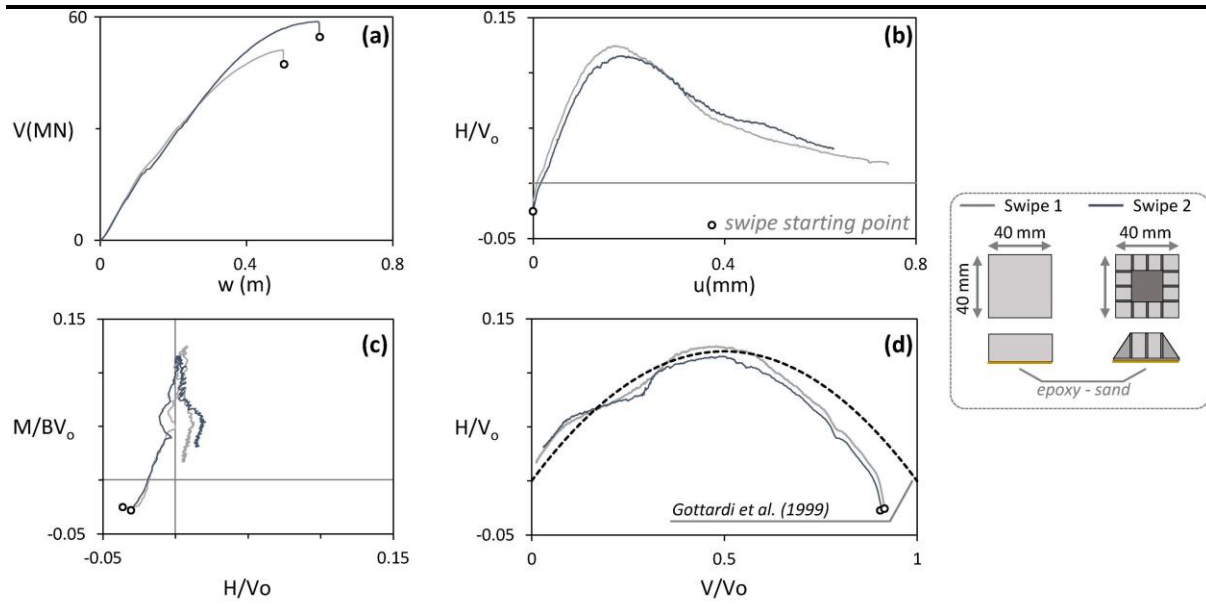


Fig. 16

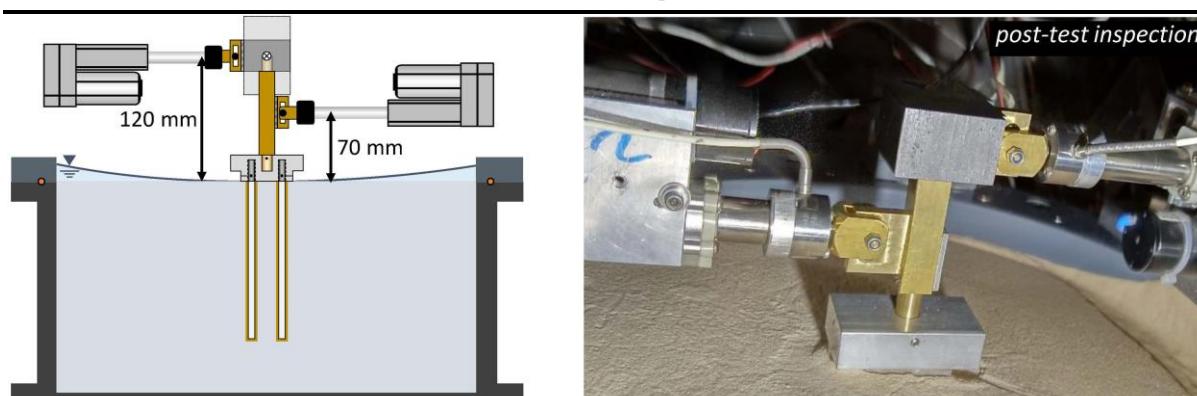


Fig. 17

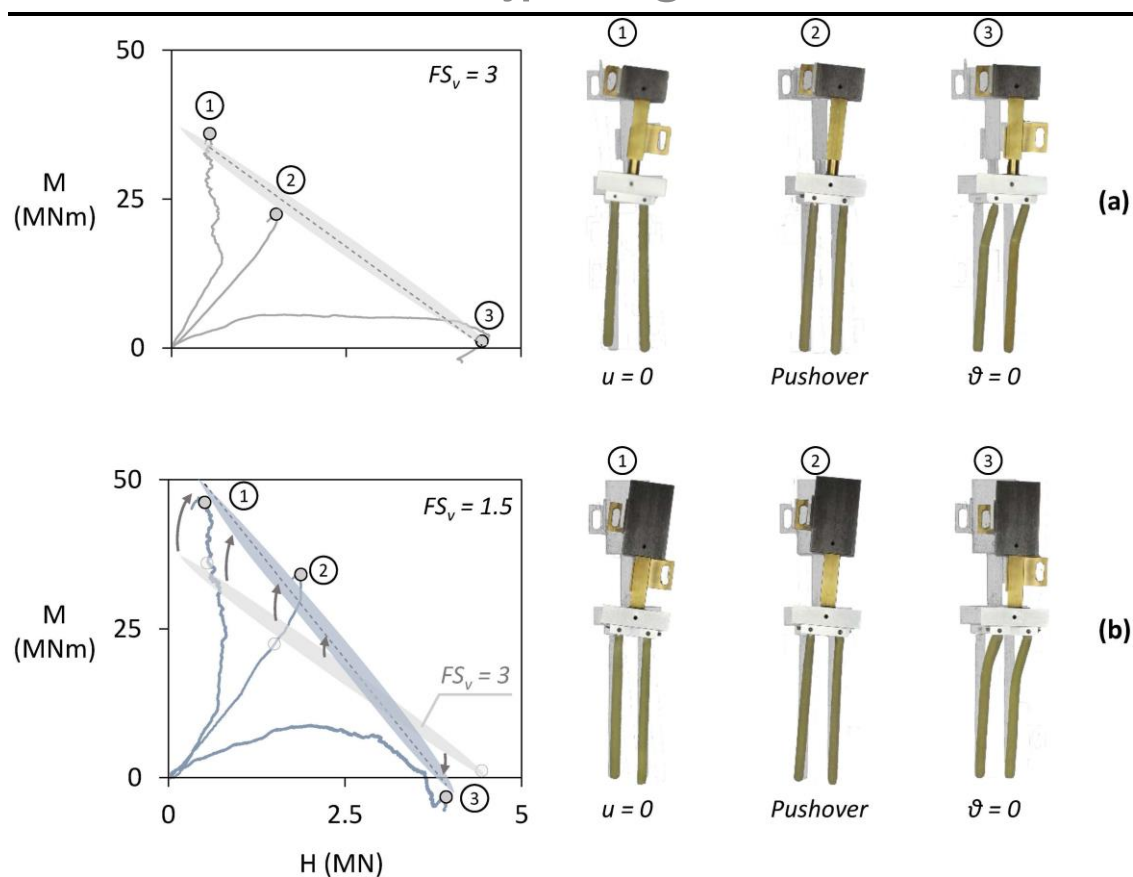


Fig. 18

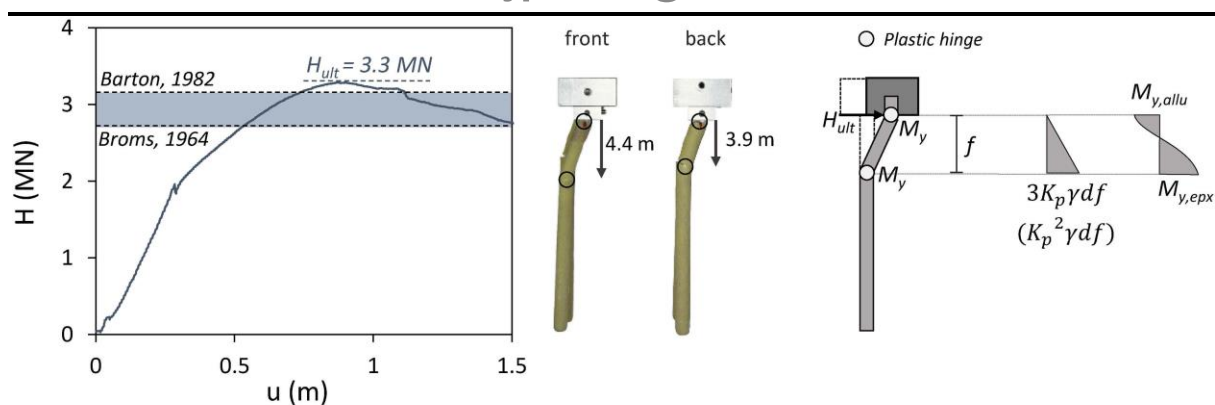


Fig. 19

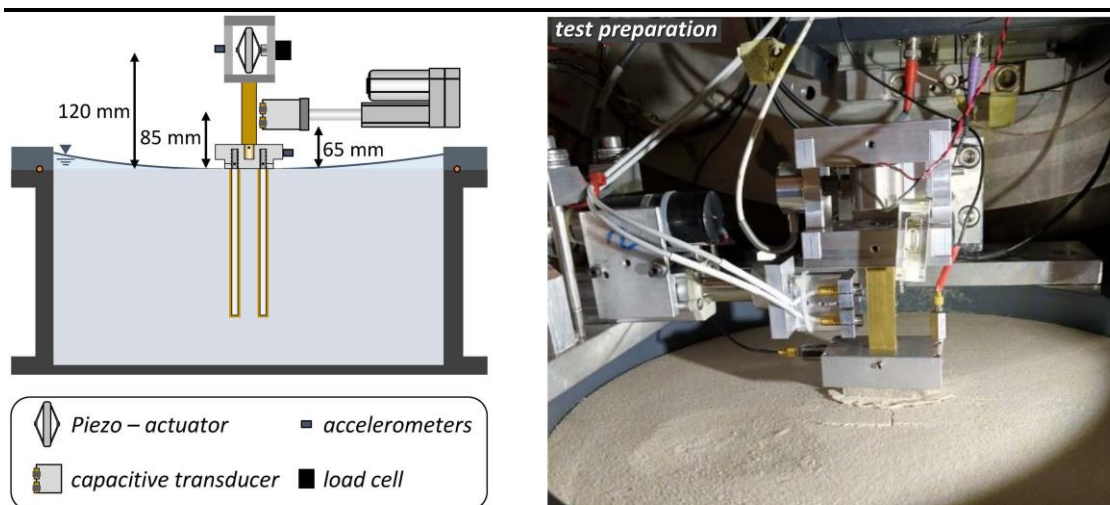


Fig. 20

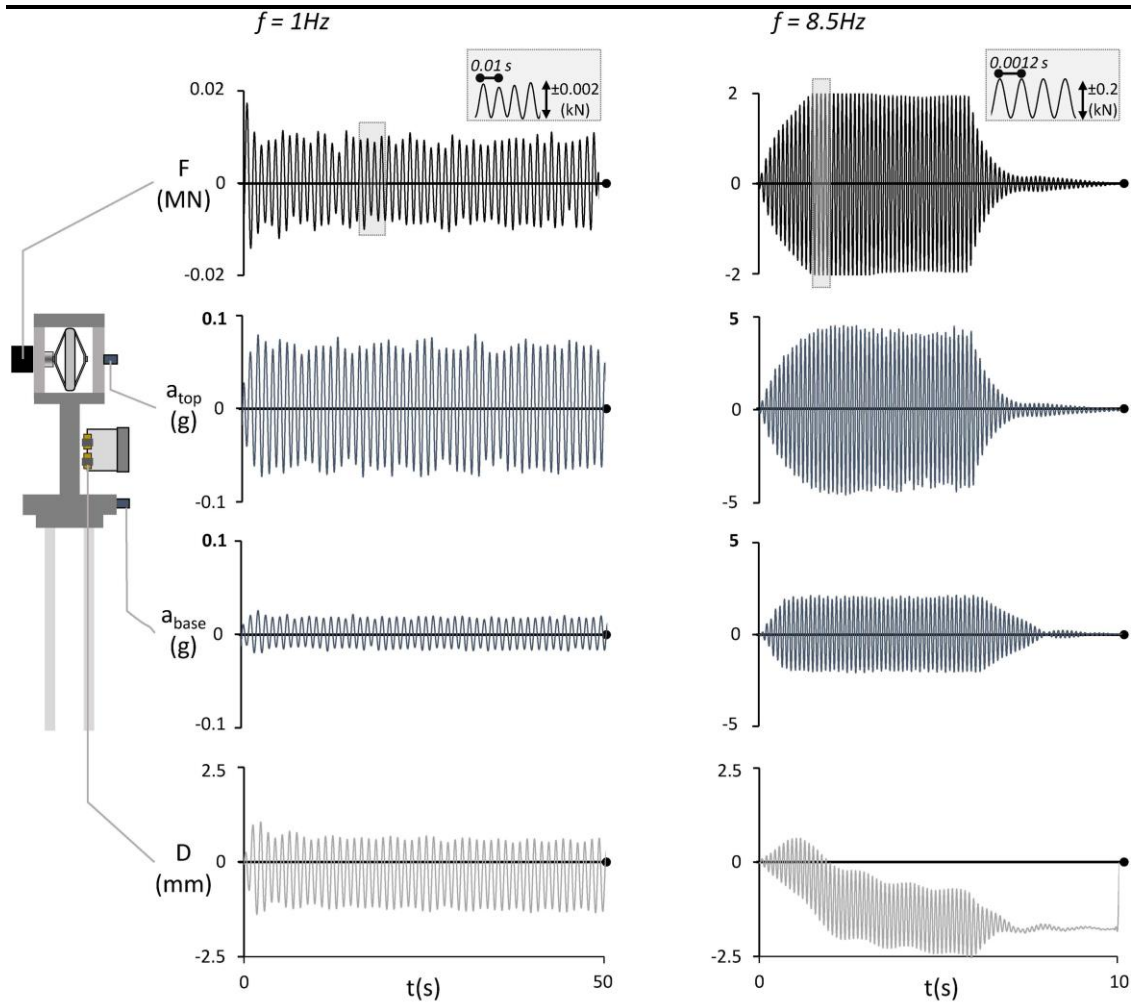


Fig. 21

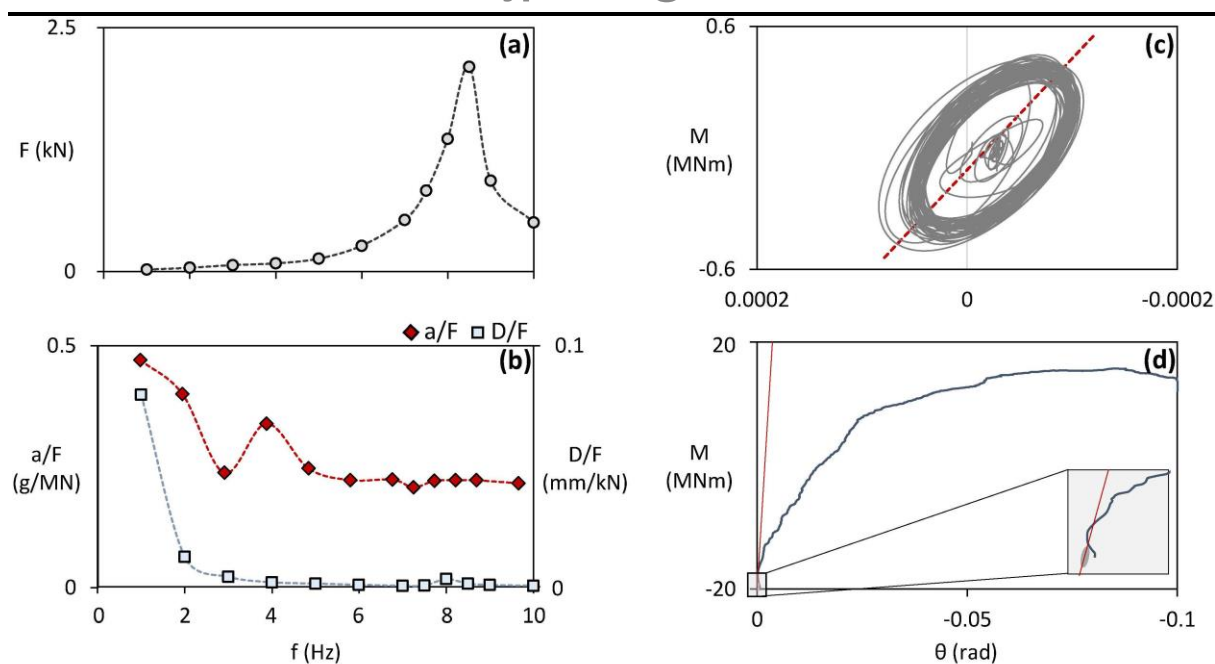


Fig. 22